Linkage of the Physical Environments in the Northern Antarctic Peninsula Region to the Southern Annular Mode and the Implications for the Phytoplankton Production

Zhaoru Zhang[1,*], Eileen E. Hofmann[2], Michael S. Dinniman[2], Christian Reiss[3], Walker O. Smith[1], Jr.[1,4] and Meng Zhou[1]

[1]. School of Oceanography, Shanghai Jiao Tong University, Shanghai, China

[2]. Center for Coastal Physical Oceanography, Old Dominion University, Norfolk, VA, USA

[3]. Antarctic Ecosystem Research Division, Southwest Fisheries Science Center, La Jolla, USA

[4]. Virginia Institute of Marine Science, William & Mary, Gloucester Pt., VA, USA

[*]corresponding author:

Zhaoru Zhang

zrzhang@sjtu.edu.cn

School of Oceanography, Shanghai Jiao Tong University, 1954 Huashan Road, Shanghai, 200030, China

Abstract

The long-term (almost 20 years) hydrographic and primary production data collected by the U.S. Antarctic Marine Living Resources (AMLR) program during the austral summer near Elephant Island and the South Shetland Islands were combined with satellite observations to assess interannual variability in environmental conditions and production of the northern Antarctic Peninsula (NAP). Correlation analyses show that interannual variability of the region is related to the dominant mode of the Southern Hemisphere extratropical climate variability, the Southern Annular Mode (SAM). Post 2000, significant correlations ($r>0.5$, $p<0.1$) are detected between SAM and environmental properties that potentially affect NAP phytoplankton production, particularly mixed layer depth (MLD), the extent of the nutrient-rich Circumpolar Deep Water (CDW), and photosynthetically available radiation (PAR). The relationship of these properties to SAM exhibits spatial variability. Near Elephant Island, interannual variations of the summertime MLD and PAR are significantly and positively correlated to the variation of the summer SAM index ($r=0.89$ and $p=0.0003$ for MLD; $r=0.64$ and $p=0.04$ for PAR). Significant correlations also exist between chlorophyll concentration and the summer SAM index ($r=0.7$, $p=0.02$), which are attributed to the SAM-related change in PAR and vertical mixing. Near the South Shetland Islands, the correlation between MLD and summer SAM index is weakened ($r=0.59$, $p=0.05$). Significant correlations are found between CDW extent and the spring SAM index as well as the annual SAM index ($r>0.7$, $p<=0.01$). Significant correlations also exist between chlorophyll concentration and the spring and annual SAM indices ($r>0.6$, $p<=0.06$). The statistical relationship between chlorophyll concentration and SAM is used with the predicted variation of SAM based on CMIP5 models to make projections of biological production change over the next 50 years in the NAP and adjacent areas. With an estimated SAM trend of 0.03 yr^{-1}, in the next 50 years the surface chlorophyll concentration over the NAP and WAP outer shelf and slope will increase by as much as 0.5 mg m^{-3}, and the integrated chlorophyll concentration over the upper 100-m water column will increase in the NAP area by 10 mg m^{-2} to 50 mg m^{-2}.

Keywords

northern Antarctic Peninsula, Southern Annular Mode, mixed layer depth, Circumpolar Deep Water, phytoplankton production

1. Introduction

The continental shelf and slope region of the northern Antarctic Peninsula (NAP, Fig. 1) is one of the biogeochemical hotspots in Antarctic marginal seas that supports abundant primary producers and higher trophic level predators (Loeb et al., 2010; Nowacek et al., 2011). It is also a major spawning and nursery ground for Antarctic krill (*Euphausia superba*) and provides an important source of krill to the Scotia Sea region of the Southern Ocean (e.g. Murphy et al., 1998; Murphy et al., 2004; Fach and Klinck, 2006; Espinasse et al., 2012). The production of the NAP region and adjacent areas is significantly modulated by environmental conditions that include vertical stratification, mesoscale circulation, light availability and sea-ice conditions (Renner et al., 2012; Zhou et al., 2013; Schofield et al., 2018). The proximity of NAP to the southern boundary of the Antarctic Circumpolar Current (ACC) allows on-shelf intrusions of the nutrient-rich Circumpolar Deep Water (CDW), which is an important modulator of the shelf ecosystem productivity (Prézelin et al., 2000; Loeb et al., 2010). Understanding variability in these physical processes is critical for projecting variability and changes in ecosystem primary production and biomass of the NAP and nearby areas.

The Antarctic Peninsula region has undergone significant climate change during the past decades (Turner et al., 2005; Thompson et al., 2011; Schmidtko et al., 2014). The major modes for the southern hemisphere (SH) extratropical climate variability, the Southern Annular Mode (SAM) and the El Niño–Southern Oscillation (ENSO), affect the atmospheric circulation (Li et al., 2015; Zhang et al., 2018), the oceanic circulation (Renner et al., 2012; Dotto et al., 2016) and the sea-ice extent (Stammerjohn et al., 2008; Simpkins et al., 2012) in this area. The SAM is characterized by opposite anomalies of sea-level pressure in the SH high and mid latitudes (Marshall, 2003), and is the dominant mode for SH extratropical climate variability. Based on numerical circulation simulations, Dinniman et al. (2012) identified a possible linkage between on-shelf CDW intrusions

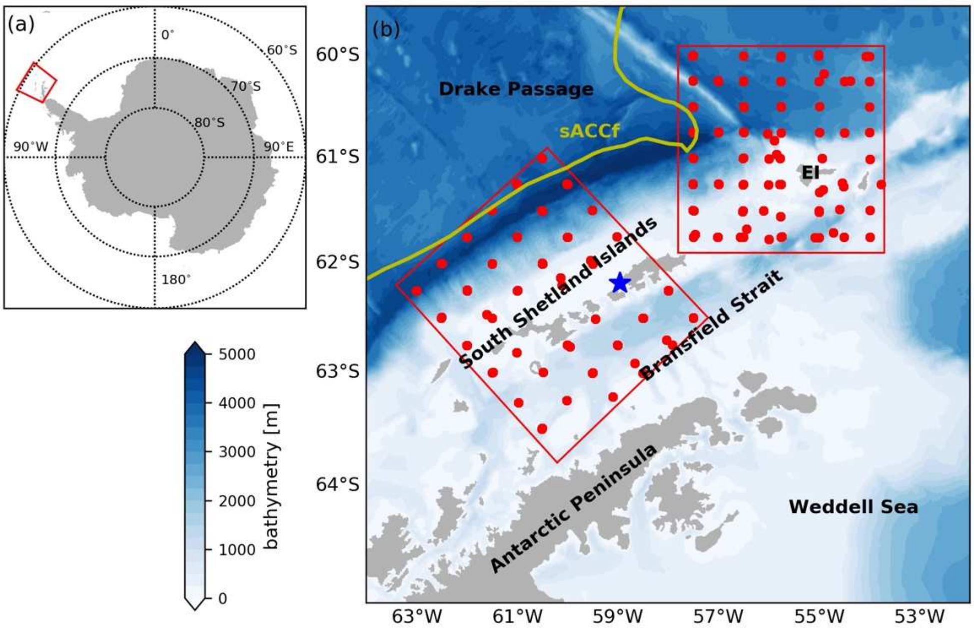

Fig. 1. (a) Location of the AMLR survey area in the Southern Ocean (red box). (b) Map of the AMLR study region in the northern Antarctic Peninsula (NAP), which includes the regions near Elephant Island (EI) and the South Shetland Islands. The AMLR survey stations for 2003 (red dots) are shown to provide an example of the sampling distribution. Boundaries of the EI and South Shetland Islands sampling grids are shown (red lines). The Bellingshausen research station (blue star) and southern Antarctic Circumpolar Front (sACCf, yellow line) are indicated.

and SAM variations for the western Antarctic Peninsula (WAP) region adjacent to NAP. Loeb et al. (2010) found that during strong La Niña years the southern ACC front moves closer to the NAP slope, favoring on-shelf intrusion of the nutrient-rich CDW, producing higher phytoplankton biomass on the shelf. Chlorophyll concentration in the upper mixed layer of NAP waters is positively correlated with the Southern Oscillation Index characterizing ENSO variability, and is accompanied by a weak correlation with mixed layer temperature (Reiss et al., 2009). Summertime primary production at a coastal site on the WAP continental shelf showed a negative correlation with SAM, which was attributed to SAM-related changes in wintertime ice formation and spring wind on upper ocean stratification (Saba et al., 2014).

These results advanced understanding of the linkage of large-scale climate modes to temporal variability in physical and ecological properties in the NAP and adjacent areas. However, such impacts may have significant spatial variability due to the complex geometry and dynamical variability of the Antarctic Peninsula continental shelf system. For example, distance to the shelf break can determine the influence of CDW intrusions (Dinniman and Klinck, 2004; Klinck et al., 2004), latitudinal location controls the effects of westerlies and sea-ice freezing and melting (Stammerjohn et al., 2008), and nutrients and micronutrients are supplied from different sources in different areas (Serebrennikova and Fanning, 2004; Frants et al., 2013; Annett et al., 2015). These variations produce different relationships between local oceanic processes and large-scale climate patterns. Also, seasonal variability can modify the phase relation between the temporal variability of the oceanic processes and the climate modes. Moreover, the temporal variability of the individual climate modes occurs with different time scales, which results in shifting dominance of a mode during different time periods.

The objective of this study is to identify and quantify the effects of the shifting relationships in large-scale climate modes, in particular SAM, on the local oceanic system of NAP. The long-term hydrographic and ecological data collected by the U.S. Antarctic Marine Living Resources (AMLR) program in the environments of Elephant Island (EI) and the South Shetland Islands (SSIs) in the NAP region (Fig. 1) are combined with satellite-derived observations to investigate the relationships between interannual variability in the physical environment and ecosystem production and SAM. This study focuses on the austral summer season when the AMLR observations are available, primary production reaches its annual maxima, and sea ice is absent in the AMLR survey area. The physical quantities of interest are mixed layer depth (MLD), the extent of CDW, and irradiance availability over the study area. All potentially affect primary production by modifying the horizontal fluxes of nutrients, the vertical supply of macronutrients and micronutrients, and photosynthetic efficiency.

2. Data and Methods

2.1. Data

The U.S. AMLR program (https://swfsc.noaa.gov/AERD-Data/) conducted standardized surveys near EI began from the early 1990s through 2011. The AMLR field seasons generally included two summer surveys, one from January to February and one from February to early March, although exceptions occurred in 2006 to 2007 and 2009 to 2011 when only one survey occurred (Reiss et al., 2009; Loeb et al., 2010). The number of stations occupied during the surveys ranged from 144 in 1994 to 48 in 2006, but the area covered by the surveys was similar among the years. Beginning in 1997, the surveys were expanded westward to include the Bransfield Strait and the shelf and slope areas north of the SSIs, and by 2001 a relatively fixed survey area near the SSIs was established (Fig. 1). The number of stations occupied in this region varied from 20 in 2010 to 75 in 2002. For this study, the EI and SSIs survey regions are analyzed separately because of the different time intervals included in the data and the different ocean dynamics in the two areas. In 2000 only a few stations were occupied in the EI and SSIs areas, and therefore, data from this year were excluded from the analysis.

At each AMLR station, hydrographic data were collected using a Sea-Bird SBE 911 system mounted on General Oceanics 12-bottle Rosette or a Sea-Bird SBE32 Carousel sampler. The CTD casts collected samples to a maximum depth of 750 m or 5 m above the bottom at locations less than 750 m, and water samples were collected at standard depths of 5, 10, 15, 20, 30, 40, 50, 75, 100, 200 and 750 m. The chlorophyll-*a* (hereafter Chl) concentration was determined by fluorometric method using a Turner Designs fluorometer. The integrated Chl concentration over the upper 100-m water column is used to indicate phytoplankton biomass in this study.

Satellite-retrieved Chl concentration data, obtained from the Moderate Resolution Imaging Spectroradiometer (MODIS) Level-3 standard mapped dataset (https://modis.gsfc.nasa.gov) with a horizontal resolution of 4 km, which are available starting in 2000, were used in the analysis. Irradiance intensity was analyzed using the MODIS photosynthetically available radiation (PAR) data. The seasonal and annual SAM indices used in this study are from the station-based Marshall SAM index that is derived from the zonal pressure difference between the latitudes of 40°S and 65°S (Marshall, 2003). Wind speed data were obtained from meteorological observations made at the Bellingshausen Station (Fig. 1), which are available at the Reference Antarctic Data for Environmental Research (READER) project website (https://legacy.bas.ac.uk/met/READER/). Antarctic ozone data were obtained from the National Aeronautics and Space Administration (NASA) Ozone Watch dataset (https://ozonewatch.gsfc.nasa.gov/meteorology/SH.html), which provides the total column ozone averaged around the polar cap for latitudes of 60°S–90°S in Dobson Units (DU).

2.2. Methods

Mixed layer depth is defined as the depth where the potential density differs by 0.03 kg m^{-3} from the surface potential density (Dong et al., 2008). The extent of CDW is indicated by the temperature distribution along the potential density surface of 27.6 kg m^{-3} (Loeb et al., 2010). The CDW extent over the study area is linked to both seasonal and annual SAM indices, with "annual" defined by the summer season (December to February for SAM indices), which coincides with the

AMLR survey season, and the autumn (March to May), winter (June to August) and spring (September to November) seasons preceding the summer.

The variables derived from the AMLR measurements were mapped onto a 21 ×21 grid (boundaries of the grid shown in Fig. 1b) using an objective analysis approach for both of the EI and SSIs regions. The grid distance varies from 8 km to 12 km. The gridded data were analyzed using empirical orthogonal function (EOF) analysis to obtain the principle component time series associated with the 1st EOF mode (PC1) of the variables. The PC1 time series were then divided by their standard deviations to obtain the normalized PC1 time series. The relationship between the variables and SAM was examined by comparing the normalized PC1 time series (hereafter we use PC1 to denote the normalized PC1 for convenience) and the SAM index. Correlation coefficients (r) and statistical significance (p-value using Wald Test with t-distribution of the test statistic; hereafter p) between each variable and SAM were obtained by linear regression. Correlations are considered as significant if $p \leq 0.1$. Variability of the different variables was analyzed by comparing their PC1 time series. The relationship obtained from the linear regression was used to project Chl concentration using a projected trend in SAM obtained from phase 5 of the Coupled Model Intercomparison Project (CMIP5) product by Zheng et al. (2013). The spatial patterns of 1st EOF modes of major variables analyzed in this study are provided in Fig. S1 and Fig. S2.

3. Results

3.1 Mixed layer depth and summer SAM

The PC1 time series of MLD in the EI region shows a weak and positive correlation (r=0.46, p=0.04) with the summer SAM index (hereafter named SAMI) over the time covered by the

AMLR observations (Fig. 2a). The 1st EOF mode explains 32.9% of the total MLD variance (Table 1). The positive correlation is most obvious after 2000 and as a result the data from 2001 to 2011 were used to analyze the relation between MLD variability and the summer SAMI. During this period, the 1st EOF mode explains 86.3% of the total MLD variance (Table 1). The MLD PC1 and the summer SAMI (Fig. 2b) are more strongly correlated (r=0.89, p=0.0003) for 2001–2011 (all correlation statistics for the period 2001–2011 in this study are also summarized in Table S1), suggesting strong co-variability of MLD with SAM in summer during this period.

Table 1. The percent (%) of the total variance in mixed layer depth (MLD), photosynthetically available radiation (PAR), Circumpolar Deep Water extent indicated by the distribution of temperature on the potential density surface of 27.6 kg m^{-3} (T_{CDW}), and chlorophyll concentration integrated over the upper 100 m (Chl-100m) explained by the 1st EOF mode in the Elephant Island (EI) and South Shetland Islands (SSIs) survey areas. The time span included in the analysis is shown.

	MLD			**PAR**	**T_{CDW}**		**Chl-100m**		
	EI		SSIs	EI	EI	SSIs	EI		SSIs
Time	90–11	01–11	01–11	01–11	01–11	01–11	90–11	01–11	01–11
% variance	32.9	86.3	89.9	66.2	34.3	48.3	55.1	50.5	40.3

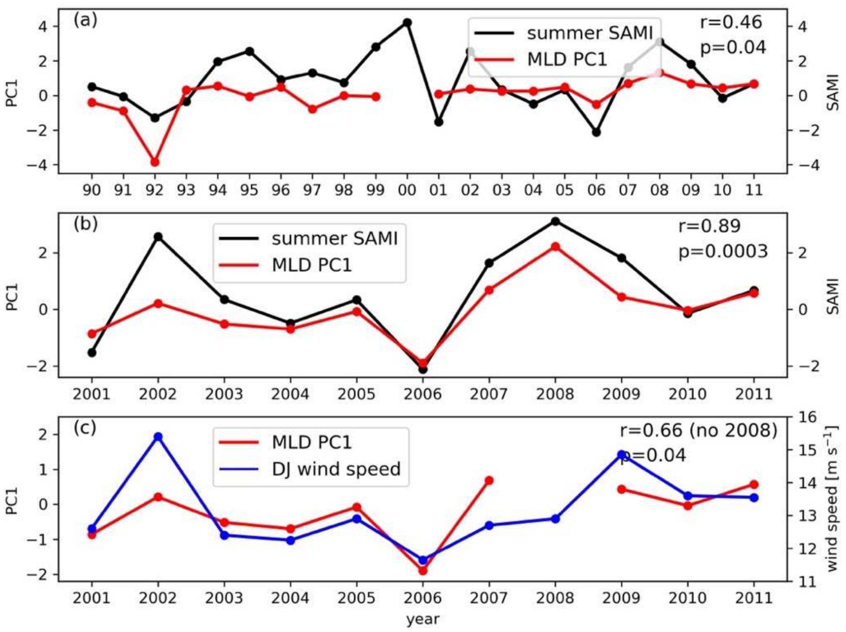

Fig. 2. (a) Time series for the Elephant Island region of the summer SAM Index (SAMI) and PC1 of mixed layer depth (MLD) calculated from the AMLR data during 1990–2011. (b) Same as (a) but for 2001–2011. (c) Time series of PC1 of MLD and the December-January (DJ) mean wind speed from the Bellingshausen Station for 2001–2011. The correlation coefficient (r) and significance level (p) for the time series are shown.

The spatial distributions of MLD in the EI region show that years with negative SAMI (Figs. 3a-d) have MLDs shallower that 40 m over the majority of this area. In years with SAMI above 1.0 (Figs. 3h-k), MLD increases to more than 60 m, and deepens to over 90 m in 2008 when SAMI has the largest positive value. Positive SAMI corresponds to strong westerly winds, and this effect was investigated by correlating the MLD PC1 time series with the summer wind speed time series from the Bellingshausen Station (Fig. 2c). A significant correlation exists between the MLD PC1 and the December-January mean wind speed (r=0.66, p=0.04) if year 2008 (characterized by low wind speed but high MLD) is removed (r=0.42 and p=0.2 if 2008 included). The wind speed was also significantly correlated with the summer SAMI (r=0.64 and p=0.05, not shown).

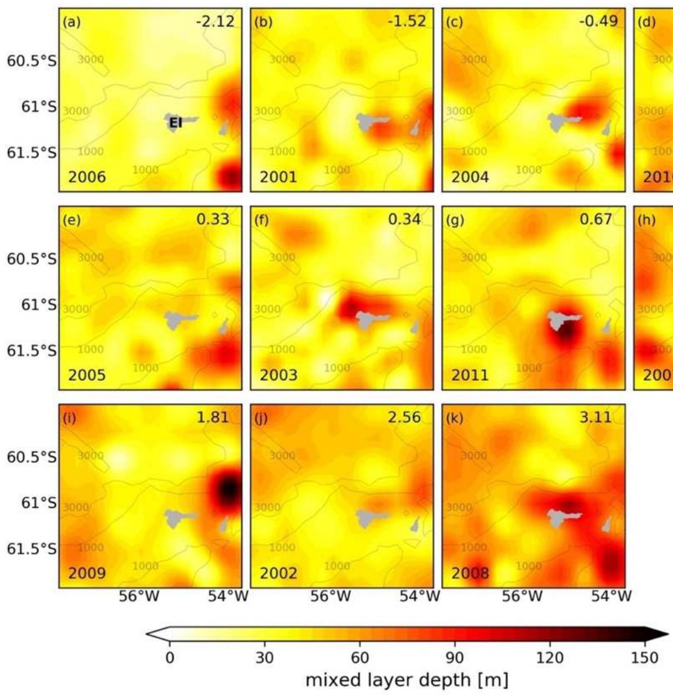

Fig. 3. Mixed layer depth distribution in the Elephant Island (EI, identified on panel a) region for 2001–2011. Years are arranged in order of increasing summer SAMI, which is shown for each year.

In the SSIs region, the 1st EOF mode explains 89.9% of the total MLD variance (Table 1). Similar to the EI region, a significant and positive correlation exists between the MLD PC1 and the summer SAMI (Fig. 4a), but the correlation is lower (r=0.59, p=0.05), which corresponds to lower correlation between the MLD PC1 and the summer wind speed (Fig. 4b; r=0.56 and p=0.1 excluding year 2009 that has high wind speed but moderate MLD; insignificant correlation if 2009 included).

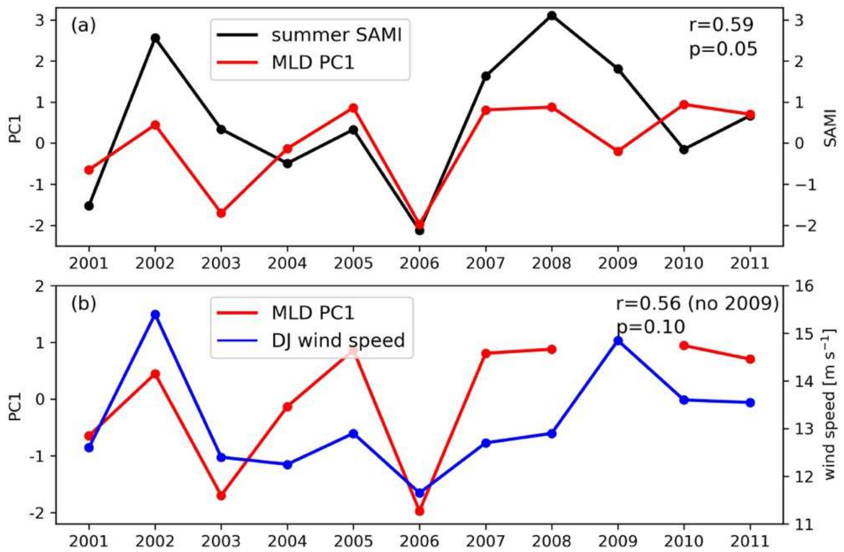

Fig. 4. Time series for the South Shetland Islands region during 2001–2011 of (a) summer SAM Index (SAMI) and PC1 of mixed layer depth (MLD) calculated from the AMLR data, and (b) PC1 of MLD and the December-January (DJ) mean wind speed from the Bellingshausen Station. The correlation coefficient (r) and significance level (p) of the correlation between the time series are shown.

3.2 Irradiance and summer SAM

The spatial distributions of PAR (Fig. 5) derived from MODIS measurements made in the EI region over 2001–2011 (MODIS data started in 2000) show that, except for 2006 and 2004, there is a general increasing trend from low-SAMI (below 1.0) years to high-SAMI (above 1.0) years. In low-SAMI years (2001, 2010 and 2005), PAR values remained around 20–25 Einstein m^{-2} d^{-1} over the study area. In all years with SAMI above 1.5 (2007, 2009, 2002 and 2008), PAR values over the AMLR survey region were above 28 Einstein m^{-2} d^{-1}. Temporal variation in PAR was 10%–20% of its mean value corresponding to the temporal variation of SAMI. PC1 of PAR over the EI region is significantly correlated with the summer SAMI excluding 2006, which has the lowest SAMI but high PAR values (Fig. 6a), and both are significantly correlated with the summer total ozone column averaged over the band 60°S–90°S (Figs. 6b and 6c). The distribution of PAR for the SSIs region is not included because extensive missing data in the southeast section of this area over nearly all years prevented meaningful analysis.

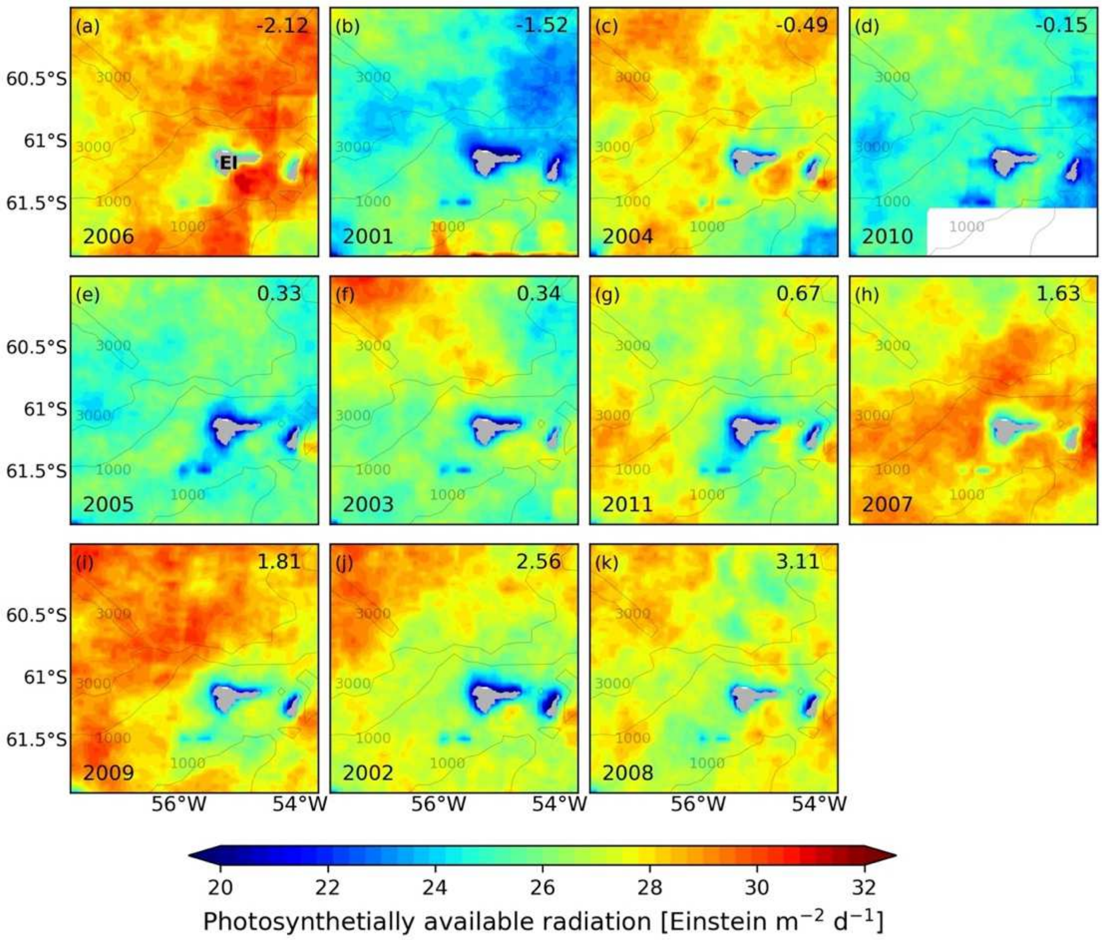

Fig. 5. Distribution of summer photosynthetically available radiation (PAR) obtained from MODIS for the Elephant Island (EI, identified on panel a) region for 2001–2011. Years are arranged in the order of increasing summer SAMI, which is shown for each year. The white area in (d) is due to a data gap in the MODIS dataset.

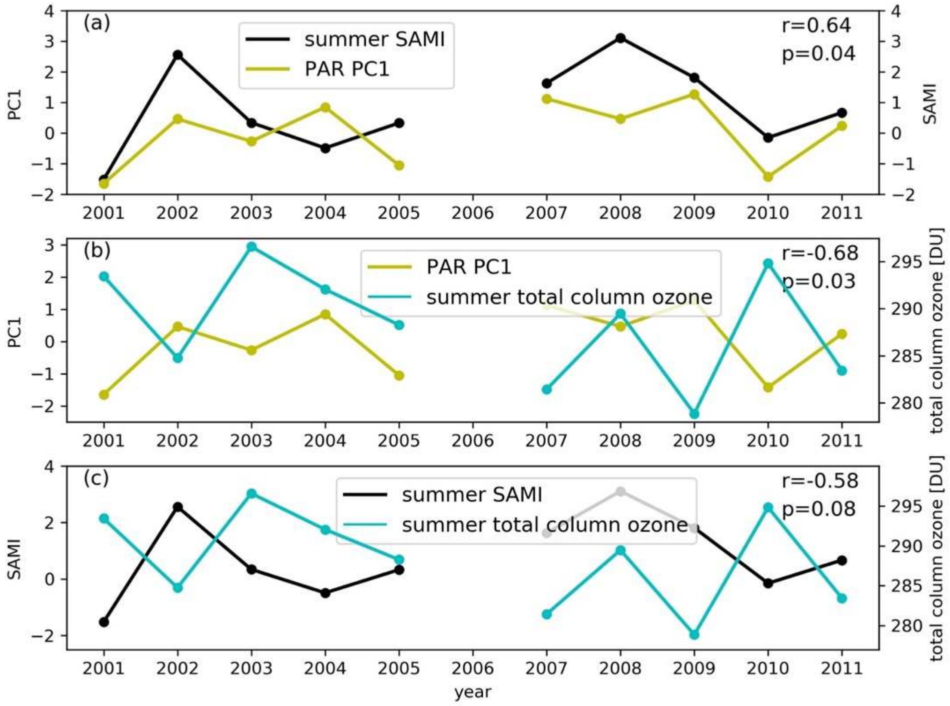

Fig. 6. Time series for the Elephant Island region during 2001–2011 of (a) summer SAMI and PC1 of photosynthetically available radiation (PAR), (b) PC1 of PAR and the total column ozone averaged over 60°S–90°S in summer, (c) the total column ozone and summer SAMI. The correlation coefficient (r) and significance level (p) of the correlation between the time series are shown. The analysis excludes 2006 that has the lowest SAMI but high PAR values.

3.3 CDW extent and seasonal and annual SAM

3.3.1 Elephant Island region

No significant correlation was found between CDW extent and summer SAMI (not shown) for the study region. Instead, significant correlations were obtained for summertime CDW extent and annual SAMI and SAMI from the preceding spring season. The extent of CDW is indicated by temperature at the 27.6 kg m^{-3} potential density surface (hereafter denoted by T_{CDW}). Larger T_{CDW} implies stronger intrusion and larger coverage of CDW in the study area. The core of CDW is tracked by the T_{CDW} range 1.5–2.0°C, and the southern boundary of CDW is tracked by the 0°C isotherm (Loeb et al., 2010) (Fig. 7).

In the EI region, years with low annual SAMI (lower than or near 0; Figs. 7a-e) are associated with northerly movement of the 0°C isotherm, and the core of CDW remained to the north of EI. In years with high annual SAMI (>1.0, Figs. 7f-j), the 0°C isotherm was displaced southwards and was not present in the study region in some years (2002, 2009 and 2011). CDW extended further south in these years and approached EI.

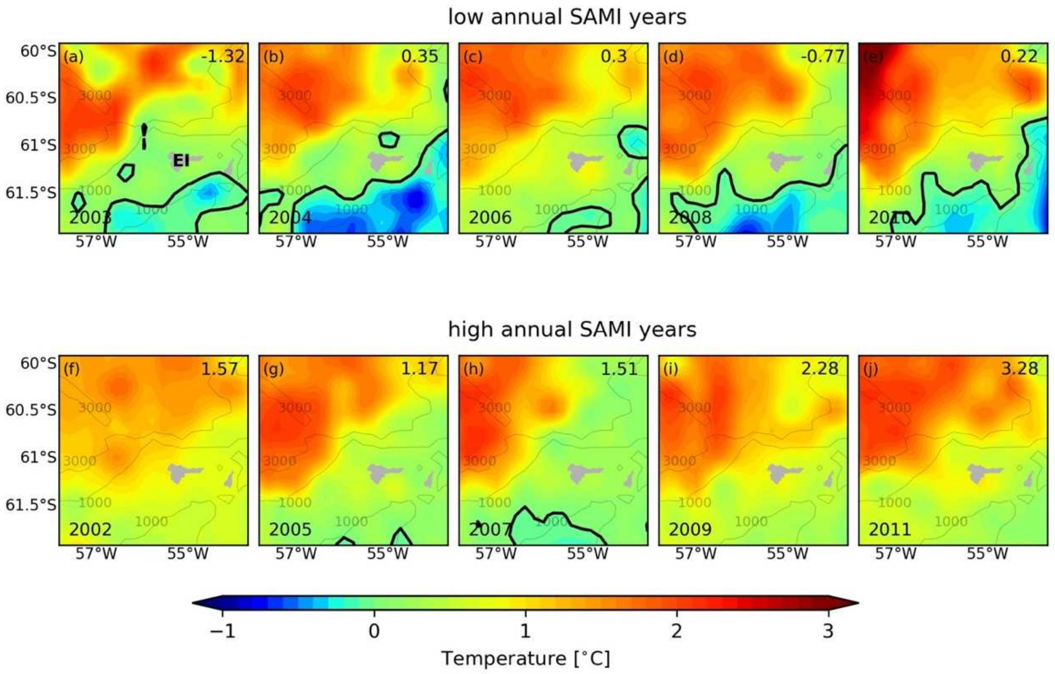

Fig. 7. Distribution of temperature on the potential density surface of 27.6 kg m^{-3} (T_{CDW}) over the Elephant Island (EI, identified on panel a) region during years with (a-e) low annual SAMI and (f-j) high annual SAMI. The 0°C isotherm (black line) and annual SAMI value in each year are shown.

Correlation of PC1 of T_{CDW} with the annual SAMI over 2001–2011 shows that CDW extent in the EI region is related to SAM variability (Fig. 8a). The 1st EOF mode explains 34.3% of the total variance of T_{CDW} (Table 1), which is significantly and positively correlated with the annual SAMI (r=0.56, p=0.08). This provides quantitative evidence for a relationship between interannual variations of CDW extent and SAM that is suggested by the temperature distributions (Fig. 7).

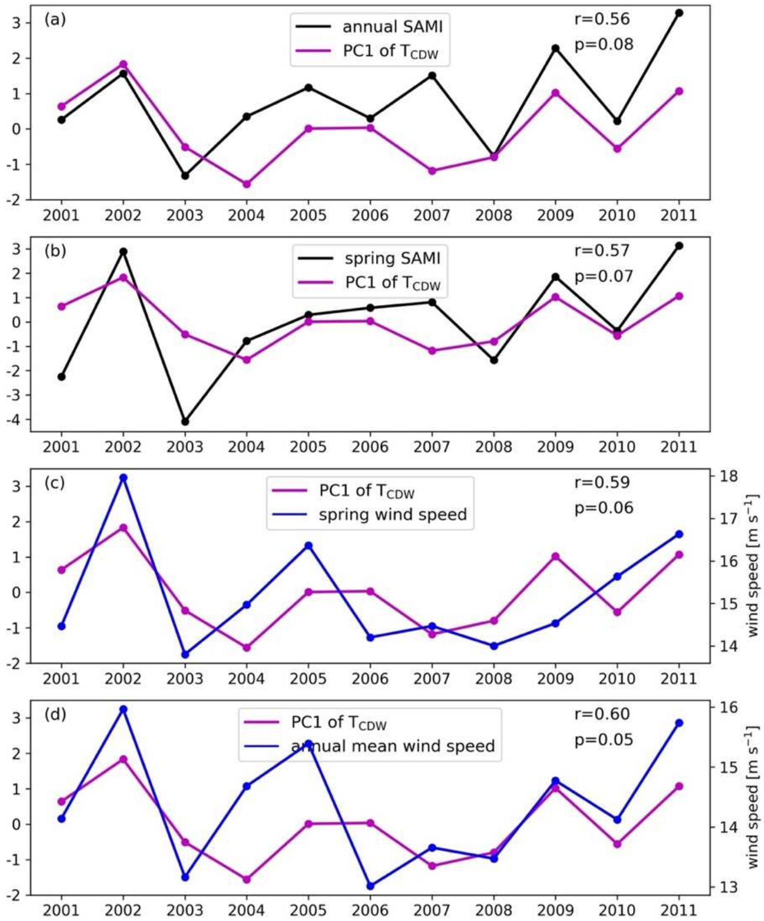

Fig. 8. Time series for the Elephant Island region during 2001–2011 of (a) annual SAMI and PC1 of temperature at the potential density surface of 27.6 kg m^{-3} (T_{CDW}), (b) spring SAMI and PC1 of T_{CDW}, (c) PC1 of T_{CDW} and the spring mean wind speed from the Bellingshausen Station, and (d) PC1 of T_{CDW} and the annual mean wind speed from the Bellingshausen Station. The correlation coefficient (r) and significance level (p) of the correlation between the time series are shown.

The correlation between CDW extent and annual SAMI was further analyzed to determine seasonal variability. Correlations of PC1 of T_{CDW} were done with SAMI time series from the autumn, winter and spring seasons preceding the summer. The only significant correlation is with the spring SAMI (r=0.57, p=0.07; Fig. 8b), which suggests that there is a lag in SAM influence on CDW distribution in the EI region.

The association between CDW intrusion and SAM results from westerly wind influence (Dinniman et al., 2012), and this was tested with correlations between PC1 of T_{CDW} and spring mean wind speed from the Bellingshausen Station (Fig. 8c). A significant and positive correlation is detected with spring wind speed (r=0.59, p=0.06; Fig. 8c), though such correlation is largely weighed by data from 2002 and 2011. This suggests that a positive SAM in spring associated with strengthened westerly wind can enhance the intrusion of CDW over the EI region. However, the significant correlation obtained with annual SAMI (Fig. 8d) allows the possibility that conditions in the previous autumn and spring affect CDW extent.

3.3.2 The South Shetland Islands region

In the SSIs region, the relationship of CDW extent with SAM is similar to that in the EI region. The extent of CDW is related to the annual SAMI (Fig. 9). Years with low annual SAMI are characterized by waters colder than 0°C occupying the southern section of the study area, while warm waters only remained in areas north of the SSIs and the shelf region shallower than 1000 m south of the SSIs (Figs. 9a, b, d and e). The exception is 2006 when water with temperatures of 0–1°C occupied the study region (Fig. 9c). High annual SAMI is associated with water warmer than 0°C covering the study region (Figs. 9f-j).

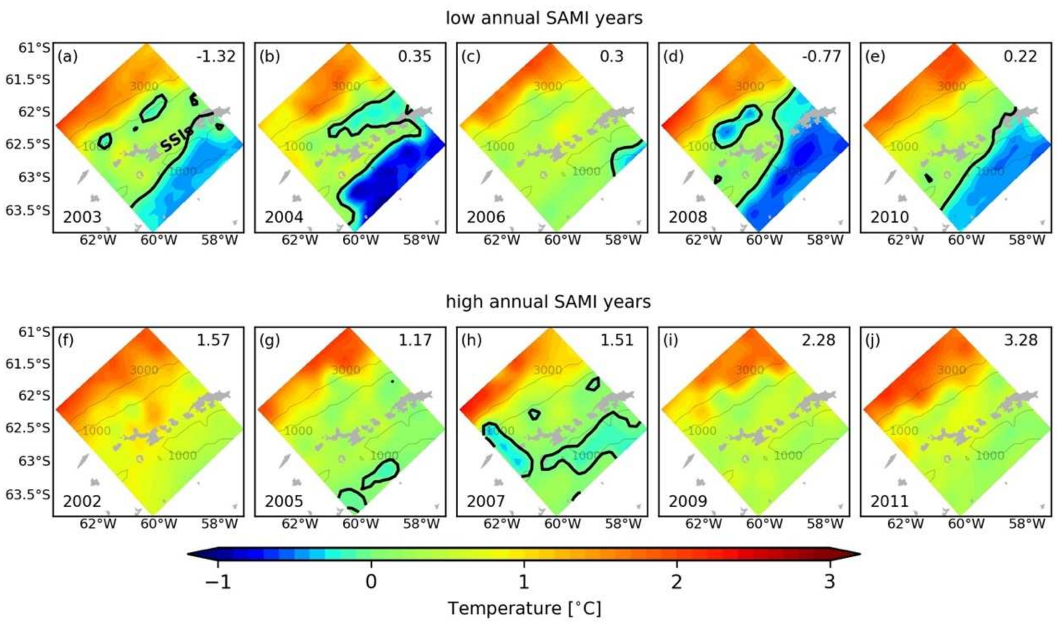

Fig. 9. Distribution of temperature on the potential density surface of 27.6 kg m^{-3} over the South Shetland Islands region (SSIs, identified on panel a) during years with (a-e) low annual SAMI and (f-j) years with high annual SAMI. The 0°C isotherm (black line) and annual SAMI value in each year are shown.

The correlation between PC1 of T_{CDW} and the annual SAMI is higher than its counterpart in the EI region (r=0.71 and p=0.01, Fig. 10a vs. Fig. 8a). The correlation between PC1 of T_{CDW} and spring SAMI is also significantly increased compared to the EI region (r=0.75 and p=0.01, Fig. 10b vs. Fig. 8b). The increase in correlation between CDW extent and spring SAMI is followed by an increase in correlation between the former and the spring wind speed (Figs. 10c),

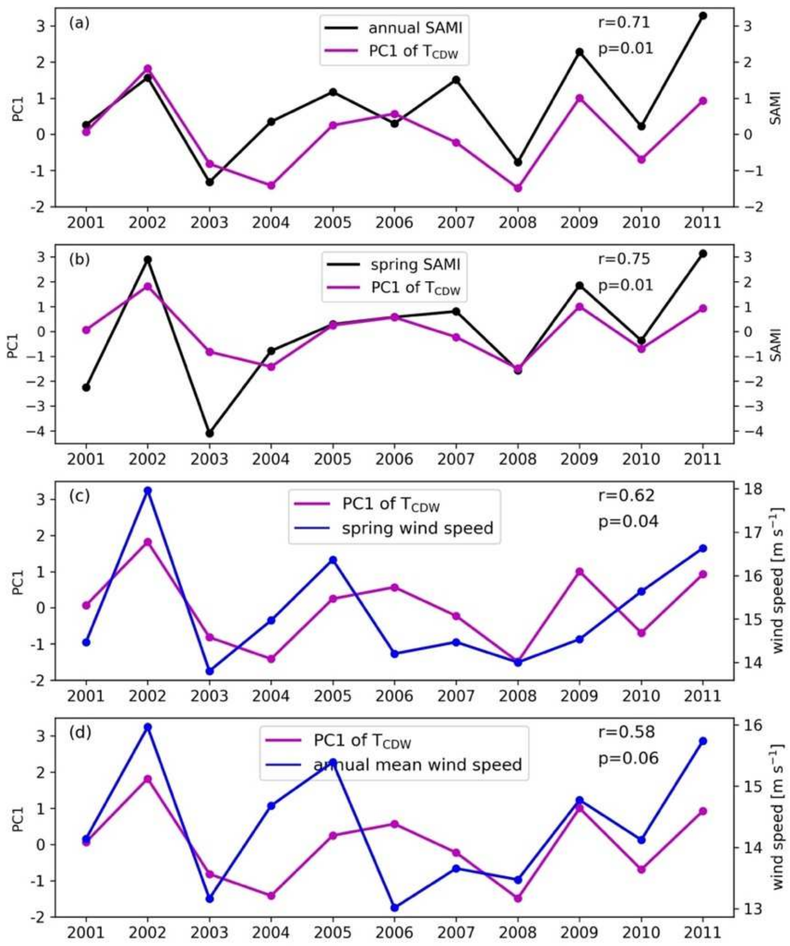

Fig. 10. Time series for the South Shetland Island region during 2001–2011 of (a) annual SAMI and PC1 of temperature at the potential density surface of 27.6 kg m^{-3} (T_{CDW}), (b) spring SAMI and PC1 of T_{CDW}, (c) PC1 of T_{CDW} and the spring mean wind speed from the Bellingshausen Station, and (d) PC1 of T_{CDW} and the annual mean wind speed from the Bellingshausen Station. The correlation coefficient (r) and significance level (p) of the correlation between the time series are shown.

though similar to Fig. 8c, the correlation between CDW extent and wind is largely dominated by data from 2002 and 2011. The correlation of CDW extent to the annual wind speed for the SSIs region is slightly reduced compared to that obtained for the EI region (Fig. 10d vs. Fig. 8d).

3.4 Chlorophyll distribution

3.4.1 Elephant Island region

The integrated Chl concentration over the upper 100 m (hereafter Chl-100m) calculated from observations provides a proxy for inferring SAM effects on the ecosystem over the period encompassed by the AMLR surveys in the Elephant Island region (Fig. 11). The low-summer-SAMI years are mostly characterized by Chl-100m concentrations lower than 60 mg m^{-2}, and the open ocean area in the northwestern section (offshore of the 3000-m isobath) had concentrations below 30 mg m^{-2} (Figs. 11a-f, h). One notable exception is 2006 (Fig. 11g) when Chl-100m concentrations exceeded 100 mg m^{-2} over a large fraction of the study area, while 1991 (Fig. 11a) is also noted for large Chl-100m concentrations above 64 mg m^{-2} over most of the region. In high-summer-SAMI years, Chl-100m concentrations above 60 mg m^{-2} occurred over most of the survey area, except for the northwestern section (Figs. 11i-p). Chlorophyll concentrations in this region remain low, but are higher relative to those in low-summer-SAMI years.

The correlation between PC1 of Chl-100m and summer SAMI is high and positive ($r=0.61$, $p=0.004$) for 1990–2011, excluding the anomalous 2006 observations that are a factor of 2 to 3 higher (Fig. 12a). The 1st EOF mode explains 55.1% of the Chl-100m variance. The correlation between PC1 of Chl-100m and summer SAMI is higher, 0.71, for 2001–2011 (Fig. 12b). Excluding the anomalous year 2006, PC1 of Chl-100m is significantly and positively correlated with PC1 of PAR and PC1 of MLD (Figs. 12c and 12d) for 2001–2011. The correlation with PAR is higher than that with MLD (r=0.75 vs. 0.60, p=0.01 vs. 0.07). No significant correlation is found between PC1 of Chl-100m and PC1 of T_{CDW} in this area.

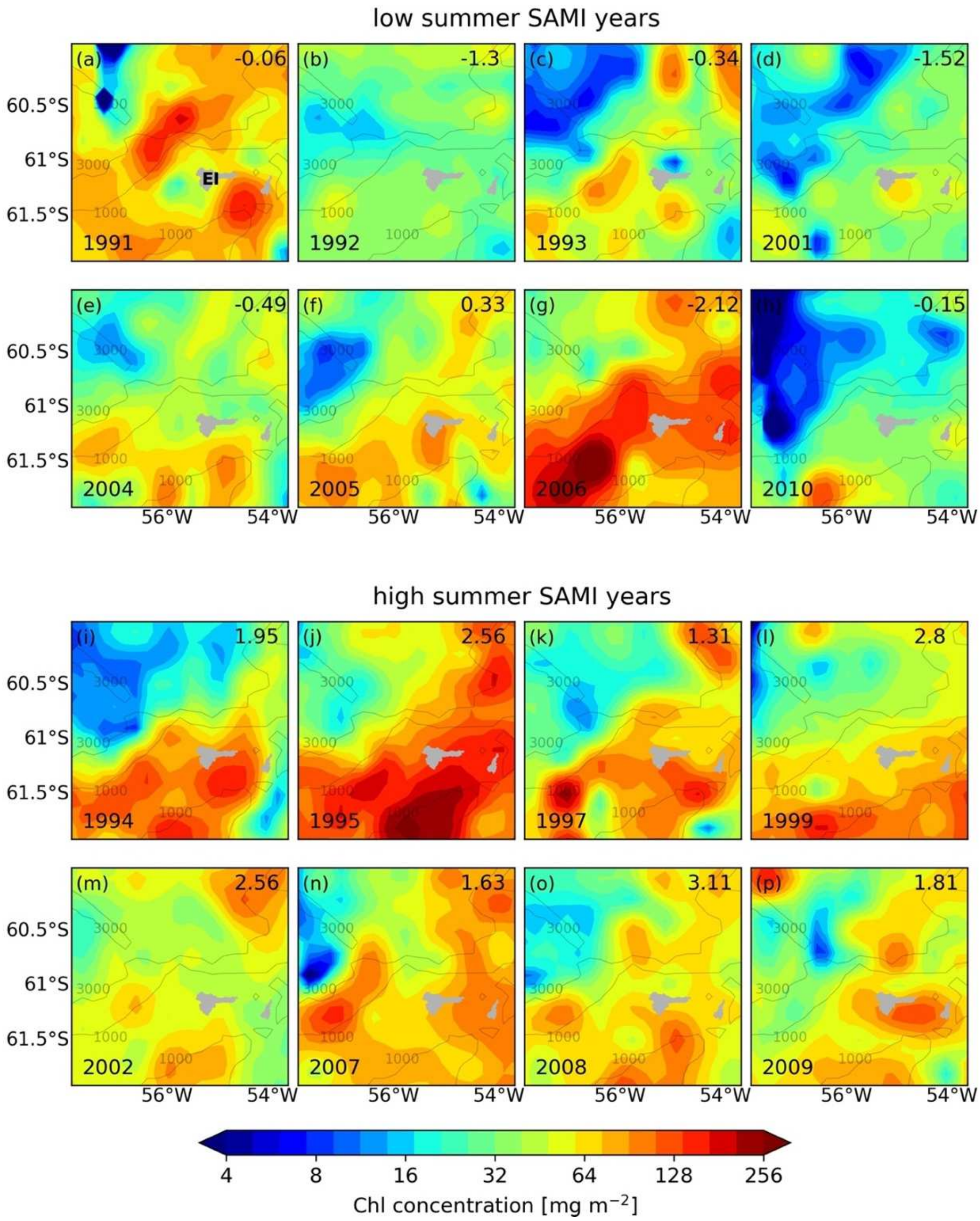

Fig. 11. Distribution of chlorophyll concentration in the Elephant Island (EI, identified on panel a) obtained by integrating the AMLR observations over the upper 100 m for years with (a-h) low summer SAMI and (i-p) high summer SAMI. The summer SAMI value is shown for each year.

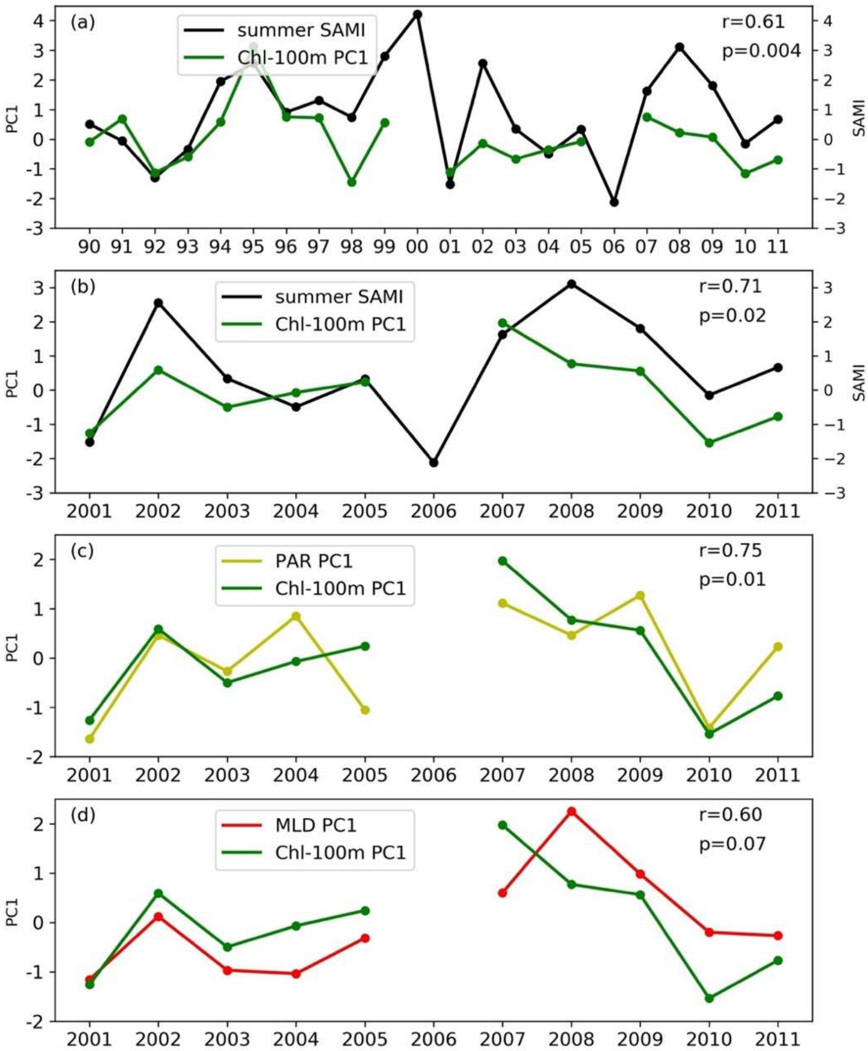

Fig. 12. (a) Time series for the Elephant Island region of summer SAMI and PC1 of chlorophyll concentration integrated over the upper 100 m (Chl-100m) for 1990–2011. (b) Same as (a) but for 2001–2011. Time series of (c) PC1 of Chl-100m and PC1 of PAR and (d) PC1 of Chl-100m and PC1 of MLD for 2001–2011. The correlation coefficient (r) and significance level (p) of the correlation between the time series are shown. The analysis excludes 2006 that has the lowest SAMI but high values of PAR and Chl-100m.

3.4.2 The South Shetland Islands region

In years with low annual SAMI (Figs. 13a-e), Chl-100m over the SSIs region were 10–60 mg m^{-2}, except for 2006 when Chl-100m were exceptionally high. For years with annual SAMI above 1.0 (Figs. 13f-j), Chl-100m over the SSIs increased to 64–150 mg m^{-2}. The correlation between PC1 of Chl-100m and summer SAMI in the SSIs region for 2001–2011 is less than that for the Elephant Island region (r=0.59, p=0.09; Fig. 14a). No significant relationship emerged between the Chl-100m PC1 and the MLD PC1 (not shown), and the large gap in PAR data availability for the region precluded investigation of a Chl-100m–PAR relationship. Compared to the summer SAMI correlation, the correlations between Chl-100m and spring and annual SAMI are higher. Excluding data from 2006 and 2011, the correlation between PC1 of Chl-100m and spring SAMI increases to 0.64 (Fig. 14b, p=0.06; the correlation is insignificant if 2011 data are included). PC1 of Chl-100m is more correlated with the annual SAMI (Fig. 14c, r=0.78, p=0.01). PC1 of Chl-100m is weakly and significantly correlated with T_{CDW} (Fig. 14d) (r=0.54, p=0.10) if data from 2006 and 2011 are excluded (insignificant if 2011 data are included), although the correlation is not as strong as that obtained with SAM.

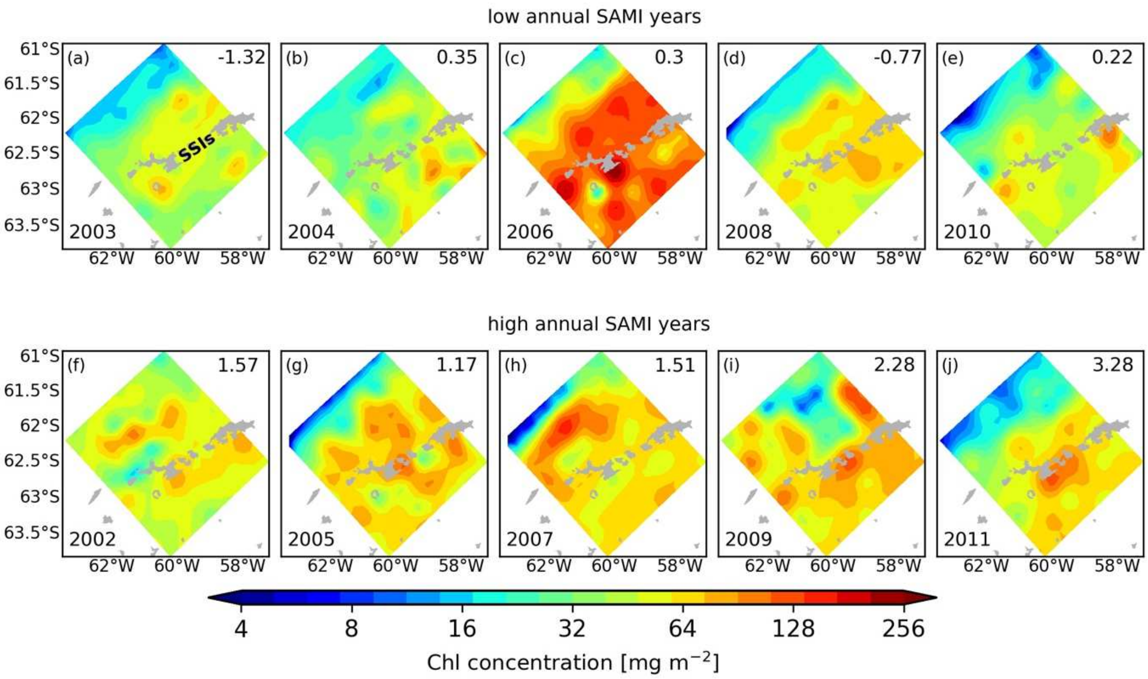

Fig. 13. Distribution of chlorophyll concentration integrated over the upper 100 m in the South Shetland Islands (SSIs, identified on panel a) region during (a-e) years with low annual SAMI and (f-j) years with high annual SAMI. The annual SAMI value for each year is shown.

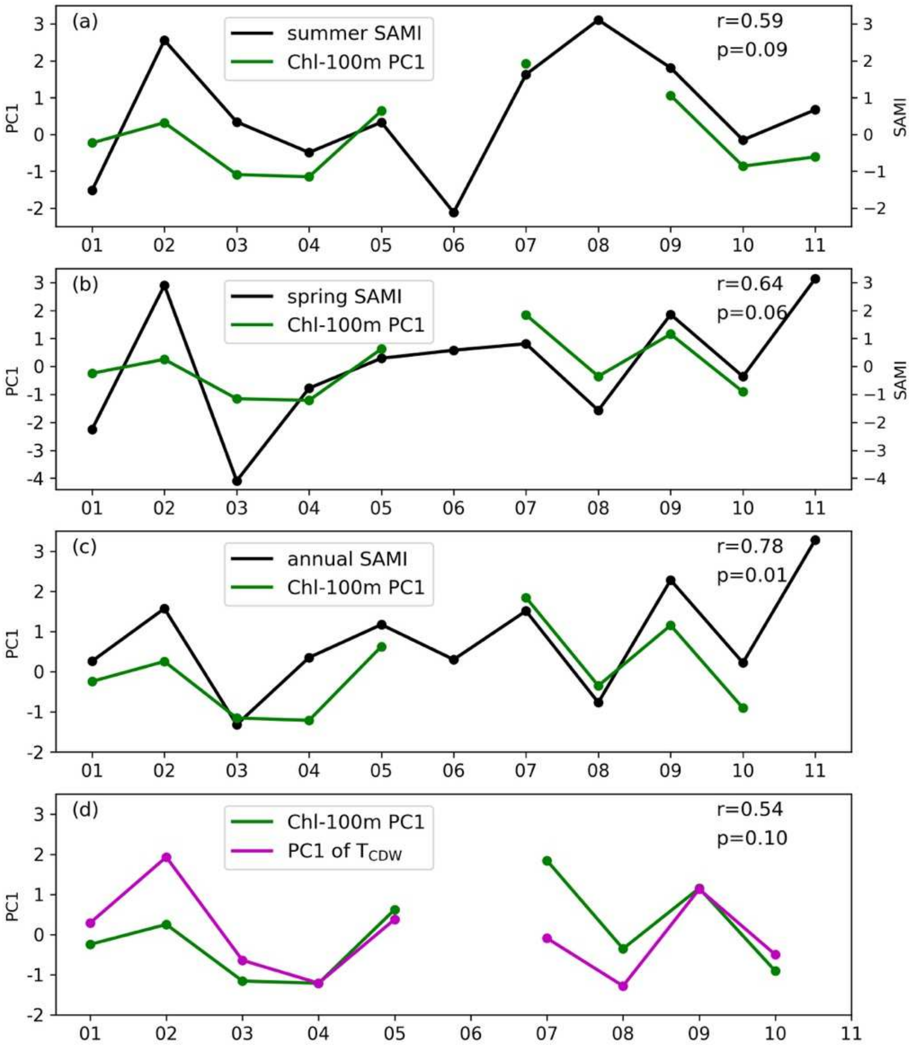

Fig. 14. Time series for the South Shetland Islands region during 2001–2011 of (a) summer SAMI and PC1 of chlorophyll integrated over 100 m (Chl-100m), (b) spring SAMI and PC1 of Chl-100m, (c) annual SAMI and PC1 of Chl-100m, and (d) PC1 of Chl-100m and PC1 of temperature on the potential density surface of 27.6 kg m^{-3} (T_{CDW}). The correlation coefficient (r) and significance level (p) of the correlation between the time series are shown. Data from 2006 were excluded from calculation of all correlations and data from 2011 were excluded from calculation of the correlations shown in b-d.

4. Discussion

4.1 Vertical mixing and chlorophyll concentration

The mixed layer depth (MLD) is affected by wind forcing and ocean-atmosphere heat fluxes. A shift in SAM towards its positive phase (corresponding to higher SAM index) increases the sea-level pressure difference between the SH mid and high latitudes, resulting in strengthened and poleward shifted westerlies (Lefebvre et al., 2004; Sen Gupta and England, 2006), which potentially enhances vertical mixing in Antarctic marginal seas. However, a positive SAM phase is also associated with strengthening of the Amundsen Sea Low, which produces stronger northwesterlies over the NAP that bring warm air from the lower latitudes to the NAP region (Lefebvre et al., 2004; Zhang et al., 2018), producing warming and enhanced precipitation, which can increase the surface stratification by atmosphere-ocean heat fluxes. The variability in MLD, and hence vertical mixing, is then a trade-off in the relative strength of the two effects. We examined the surface temperature patterns over the study areas and did not find notable differences between the high and low SAMI years (not shown), suggesting that air-sea fluxes are not a dominant factor for the MLD variation. The significant positive correlations between summer wind speed and MLD in the EI and SSIs regions also support that wind is the major factor linking the MLD and SAM variability. Wind-induced Ekman convergence or divergence can result in downwelling or upwelling, which will increase or decrease the MLD. Temperature profiles along cross-shelf transects were examined and no significant trend in upwelling or downwelling with increasing SAMI was detected, indicating that convergence and divergence would not play a significant role in the relation between MLD and SAM.

The effect of vertical mixing on chlorophyll concentration in the NAP is a balance between irradiance availability and the provisioning of nutrients to the upper ocean. Light limitation has been identified as an important factor controlling spring primary production (Arrigo et al., 2010; Joy-Warren et al., 2019). Positive SAM has been related to Antarctic ozone mass deficit (Arblaster and Meehl, 2006; Polvani et al., 2011), which can increase the intensity of visible light reaching the surface (Hamre et al., 2008). The significant positive correlations between PAR and SAMI with Antarctic ozone mass provides support for increased light delivery to the sea surface during the positive SAM phase, although the mechanism linking PAR and SAM variability is not fully understood. Cloudiness is likely a component of this correlation, but cloudiness data sufficient to describe this relationship are not available for the NAP region. The increased PAR under positive SAM shift in turn supports enhanced levels of chlorophyll production.

The significant positive correlations obtained between Chl-100m, MLD, and summer SAMI for the EI region support the contention that a shift in SAM towards its positive phase results in enhanced vertical mixing (deeper MLD) that potentially provides macronutrients and the micronutrient – dissolved iron, to surface waters. The associated increased PAR over the EI region can mitigate the effect of reduced light availability resulting from increased mixing.

Dissolved iron (dFe) has been shown to be a key limiting factor for primary production in Antarctic marginal seas including the NAP region (Measures et al., 2013; Jiang et al., 2019). On the NAP continental shelf, dFe concentrations are generally high (above 0.5 nM; Ardelan et al., 2010; Measures et al., 2013) and not considered as a limiting factor for primary production. However, in recent years studies found that dFe values can have significant spatial variability in the NAP and nearby WAP shelf areas due to heterogeneous biological production and iron sources. For example, Sanchez et al. (2019) detected low dFe concentrations (0.02-0.19 nM) at coastal stations west of EI. Also, Annett et al. (2017) found for the WAP area that abuts the AMLR study region, that high dFe concentrations are present at coastal stations, but low concentrations (< 0.1 nmol kg^{-1}) were widespread in mid- to outer-shelf surface waters, indicating possible iron limitation of shelf primary production. Sediments can be a major source of iron in the NAP region (Measures et al., 2013), suggesting that enhanced vertical mixing could have a role in supplying more dFe from deep waters rich in dFe to the surface layers. As shown in Frants et al. (2013) and

Measures et al. (2013), the ferricline in the open ocean near the EI and SSIs regions varies from 40 m to 120 m, and therefore stronger vertical mixing can mitigate the dFe limitation in surface water and enhance productivity. Tagliabue et al. (2014) also showed that winter deep mixing is efficient in entraining dFe from deep waters into surface water in the Southern Ocean, and this process is active near the Antarctic Peninsula. These scenarios provide a direct link between large-scale climate variability and local biological production.

Significant correlations between summer SAMI and Chl-100m and between MLD and Chl-100m were not obtained for the SSIs region, rather Chl-100m was significantly correlated with annual SAMI. Chlorophyll concentrations in the autumn, winter and spring seasons preceding the summer season are limited by light and are low (MODIS data, not shown), so iron supplied to surface water by the strong vertical mixing in these seasons may not be fully utilized and could accumulate and contribute to summer primary production. Similarly, the biomass produced in spring by the winter iron supply could be retained in the summer, contributing to the high summertime Chl concentration. Therefore, the correlation between summertime Chl-100 m and annual SAMI may reflect the integrated effect of enhanced vertical mixing over the year which controls the cumulative inputs of dissolved iron to surface waters or cumulative biomass. On the other hand, in the SSIs region significant correlations between Chl-100m and autumn and winter SAMI were not found and the correlation with spring SAMI is lower than that for annual SAMI. This implies that chlorophyll concentrations in this area also respond to other processes, such as CDW intrusions, and that it is the interactions of these processes that control the seasonal concentrations (Loeb et al., 2010). For the shelf north of EI, Zhou et al. (2013) showed that surface iron can be transported to the open ocean by the interaction of a southward meander of ACC with the shelf. With this active transport, surface iron may not accumulate in this region. Supply of summertime surface iron is then by vertical mixing in this season, which may explain the high correlation of Chl-100 m in the EI region with summer MLD and summer SAMI relative to the SSIs region. Renner et al. (2012) suggested that connectivity between the Weddell Sea and the NAP region in the upper ocean is restricted during positive phases of SAM by the stronger westerlies and poleward shifts of ACC fronts. As transport from the Weddell Sea is reduced, the open ocean northeast of EI may be more affected by surface iron-rich waters transported from the EI and SSI shelf areas. This provides another mechanism that links the Chl variability and SAM variability for the region northeast of EI.

Another aspect of deeper vertical mixing potentially counters the positive effect of iron addition. That is, when waters below the mixed layer are entrained into the mixed layer, surface phytoplankton are "diluted", as waters below the mixed layer generally have less chlorophyll than those above. This effect occurs during weather events such as cyclones or storms. While this effect may have occurred, it is not observed in the analyses because the AMLR data are composites spanning two to three months and the satellite composites are seasonal means, thereby, masking short-term effects of episodic mixing.

4.2 Associations of CDW extent with chlorophyll concentration and with SAM

Prézelin et al. (2000) and Prézelin et al. (2004) found that the hot spots of primary production in the WAP shelf area coincided with the presence of CDW. These hot spots are also characterized by low $Si(OH)_4 : NO_3^-$ ratios resulting from preferential removal of $Si(OH)_4$ by diatoms. Vertical mixing can bring water with high $Si(OH)_4 : NO_3^-$ ratios, derived from CDW, to the upper ocean, where it becomes available to phytoplankton. Alderkamp et al. (2012) and Gerringa et al. (2012) identified modified CDW (MCDW) as a dFe source for coastal areas in the Amundsen Sea. Arrigo et al. (2018) showed that high concentrations of nitrate and phosphate from

CDW were provided to upper ocean waters in non-shelf regions near the WAP, which were then entrained into surface water by winter deep mixing, creating high macronutrient concentration required to sustain the spring blooms. These processes potentially contribute to the correlation between Chl-100 m and CDW extent in the SSIs region.

Numerical circulation modeling studies suggested that the ACC transport is positively correlated with SAM via change in westerlies (Hall and Visbeck, 2002; Yang et al., 2007;), and enhanced ACC transport favors increased CDW transport onto WAP shelves (Dinniman et al., 2012). Meredith and Hogg (2006) and Screen et al. (2010) suggested that ACC mesoscale eddy activity during positive SAM phases facilitates the on-shelf intrusion of CDW. Whether the SAM can lead to a meridional shift of the ACC is in dispute (Gille et al., 2016). The AMLR survey region extends almost to the southern edge of ACC, making it difficult to analyze the above processes. However, variability in mesoscale eddy activities and ACC position related to SAM variations may contribute to the significant correlations between CDW extent and SAM but relatively weak correlations between the former and wind as shown in Fig. 10.

In the EI and SSIs regions, the lagged correlation between CDW extent and SAMI (CDW extent in summer is correlated with the preceding spring SAMI) implies that the positive SAM shift in spring enhances CDW intrusion via strengthened westerlies that promote deep-water upwelling along the slope or ACC transport. The time scale for the intruded CDW to spread over the shelf region is about three months This finding is consistent with the numerical circulation model results from Graham et al. (2016), which showed that 60–90 days is needed for the intruded CDW to spread over the shelf regions of NAP and WAP.

4.3 Spatial and temporal variations of the relationship between oceanic properties and SAM

4.3.1 Spatial variability

The Antarctic Peninsula region is influenced by the ACC, waters from the Weddell Sea and the marginal seas along West Antarctica as well as the seasonal advance and retreat of sea ice. The complexity of these interactions produces significant spatial variability of the oceanic processes and their association with large-scale climate patterns. Saba et al. (2014) found a negative correlation between summer primary production and SAM from the preceding winter and spring for the northern part of the west Antarctic Peninsula continental shelf (Palmer Station, 64.8ºS, 61.4ºW) based on observations spanning 21 years. This negative correlation results from reduced summer stratification that is produced by reduced winter sea-ice formation (thus less ice melting in summer) and stronger westerlies under positive SAM. The reduced stratification is unfavorable to primary production because of shorter retention times of phytoplankton in the euphotic layer and dilution of surface dissolved iron concentrations, which originate from glacier melt water and are surface concentrated (Annett et al., 2015).

The correlations obtained for the EI and SSIs regions in this study differ from that found by Saba et al. (2014) because of differences in vertical mixing, nutrient supply, and the effects of CDW intrusions. The EI and SSIs regions are located at more northerly latitudes and are less affected by sea ice conditions and have longer periods of open water, which affects MLD and vertical mixing. Dissolved iron in the EI and SSIs regions is mostly supplied from sediments (Measures et al., 2013). As a result, the enhanced vertical mixing associated with a shift toward positive SAM has opposite effects on mixed layer dissolved iron concentrations. Vertical mixing enhances surface dissolved iron concentration in the EI and SSIs areas and dilutes those along the Antarctic Peninsula, thereby producing opposite Chl-SAM relations for the two areas.

The EI and SSIs regions are close to the southern boundary of the ACC and are more easily influenced by CDW intrusions. This effect is evidenced by the positive significant correlations between Chl-100m, CDW extent and SAM obtained in this study. However, this correlation shows spatial variability within these regions, with summertime CDW extent being more strongly linked to the spring and annual SAM for the SSIs region than the EI region. Also, a significant correlation between summer Chl-100m and CDW extent was found for the SSIs region but not for EI. This spatial variability results from the pattern of CDW intrusions onto the NAP and nearby WAP shelf, which occur at locations with curving bathymetry, particularly the trenches located southwest of the SSIs (Dinniman and Klinck, 2004; Graham et al., 2016). These conditions occur along the SSIs shelf and CDW intrusions have more of an influence on this region. The EI region is influenced by CDW extent, but this region is also influenced by waters from the Weddell Sea (Gordon et al., 2000; Dotto et al., 2016; Du et al., 2018). Dotto et al. (2016) found that salinity in the deep waters of the central and eastern basins of the Bransfield Strait is negatively correlated with SAM, possibly due to weakened Weddell Sea coastal currents during positive SAM phases, which reduce the transport of salty shelf waters in the Weddell Sea to the Bransfield Strait. The multiple influences of SAM on deep water properties near EI can blur the correlations between CDW extent and SAM in this region.

4.3.2 Temporal variability

Significant correlations of MLD or CDW extent with summer/spring SAM in the EI and SSIs regions occurred only after 2000 and persisted for 2001 to 2011. Similar responses of ocean and sea-ice variables in the Southern Ocean with the positive phase of SAM and the negative phase of ENSO (i.e., La Niña) have been found (e.g., Simpkins et al., 2012; Ruiz Barlett et al., 2017), which make separating the effects of SAM and ENSO difficult. For example, the in-phase relation between positive SAM and La Niña has decadal variations as well as seasonal dependence (Ciasto et al., 2015; Yu et al., 2015). In the late 1990s, ENSO transitioned from an Eastern-Pacific (EP) to a Central-Pacific (CP) type (Yeo and Kim, 2015), which was followed by a similar decadal variation in the ENSO-SAM relationship. Yu et al. (2015) showed that in austral spring, only the CP-ENSO can excite SAM, so a significant ENSO-SAM relation only existed after the late 1990s. Ciasto et al. (2015) found the opposite for austral summer, with significant correlations between ENSO and SAM occurring before the late 1990s during the EP-ENSO period, but not thereafter.

Correlations between the oceanic variables and ENSO, represented by the Multivariate ENSO Index (MEI), provide an analysis of ENSO-SAM interactions in the study areas. The correlations of PC1s of MLD, CDW extent and Chl-100m with seasonal MEI for 2001–2011 show insignificant correlations for MLD and Chl-100m for both regions (Table 2), although correlations with SAMI were significant. The CDW extent is significantly correlated with spring MEI in the EI region. These results are consistent with the analysis of Yu et al. (2015) and Ciasto et al. (2015) which showed that after 2000, the ENSO-SAM relationship is weak in summer and significant in spring. However, the weak correlation between CDW extent in the SSIs with spring MEI is an exception.

Table 2. Correlation coefficients between mixed layer depth (MLD), Circumpolar Deep Water extent indicated by the distribution of temperature on the potential density surface of 27.6 kg m^{-3} (T_{CDW}), and chlorophyll concentration integrated over the upper 100 m (Chl-100m), and seasonal multivariate ENSO index (MEI) for the Elephant Island (EI) and South Shetland Islands (SSIs) survey regions. Numbers not calculated are denoted by the minus sign. Correlations that are significant ($p \leq 0.1$) are highlighted in bold.

	MLD		**T_{CDW}**		**Chl-100m**	
	EI	SSIs	EI	SSIs	EI	SSIs
summer MEI	-0.25	0.03	-	-	-0.01	-0.04
spring MEI	-	-	**-0.56**	-0.4	-	-0.15

This analysis indicates that in summer, the effect of SAM on the oceanic processes in the NAP area from 2001 to 2011 is independent of ENSO, since the effect of the latter is insignificant in the study region. This suggests that future research work investigating climatic control of dynamical and marine ecosystems in the NAP area and Southern Ocean regions should focus more on SH high-latitude climate modes, rather than remote tropical modes like ENSO (Martinson et al., 2008; Reiss et al., 2009; Loeb et al., 2010). Before 2000, the remote control from tropical processes on the SH high-latitude climate found by Ciasto et al. (2015) potentially affected correlations of oceanic quantities in the NAP with SAM.

The Chl-SAM relationship identified 2006 as an anomalous year, characterized by low summer and annual SAMI but high Chl-100m values. The anomalous high PAR values in 2006 could have resulted in the high Chl concentration. The relation between CDW extent and SAM was also anomalous in 2006 for both of the EI and SSIs regions, with warm water occupying a larger fraction of the study area relative to other low-SAMI years. Therefore, the strong CDW intrusion in 2006 may have contributed to the high biomass in this year.

4.4 The relationship between biological production and SAM and projections of future conditions

Satellite-derived measurements of surface Chl concentration allow expanding the correlation obtained between chlorophyll concentration and SAM for the AMLR study region to a larger area. Also, the extended temporal coverage of the satellite observations after 2000, relative to the AMLR observations, allow testing the Chl-SAM relationship over a longer time scale. The outer shelf and slope region inshore of the 2000-m isobath in the NAP and nearby WAP region was used to test the Chl-SAM relationship because of the availability of satellite data; the analysis then allows application of the relationship to a different area (Fig. 15a).

For the MODIS period, 2000–2018, significant and positive correlations were obtained between the interannual variation of area-averaged surface Chl concentration and spring (r=0.47, p=0.02; Fig. 15b) and annual SAMI (r=0.66, p=0.002; Fig. 15c). Setting the offshore boundary of the selected region at the 1000-m isobaths yields higher correlation coefficients, 0.54 and 0.70 for spring and annual SAMI respectively, similar to those obtained for the SSIs region. These correlations suggest that oceanic processes are linked to SAM over a broader region of the continental shelf and slope of the Antarctic Peninsula.

Although significant correlations were not found between the hydrographic properties and SAM for the EI region before 2000, Chl-100m in this region is significantly correlated with the summer SAMI throughout the AMLR observational period 1990–2011 (Fig. 12a). The Chl-summer SAM correlation prior to 2000 may arise from the co-variability of PAR and the summer SAM, but this hypothesis cannot be verified because of the lack of PAR data for this time period. The robust Chl-SAM correlation in the AMLR survey area, together with the robust correlation between annual SAMI and Chl concentration over the NAP and WAP continental shelf and slope in 2000–2018 was used to project primary production, represented by chlorophyll concentration, associated with projected changes in SAM. Variability in SAM results from Antarctic ozone mass and greenhouse concentration (Shindell and Schmidt, 2004; Arblaster and Meehl 2006). Using the output of 12 models from the CMIP5 product, Zheng et al. (2013) estimated the trend in SAM for the 21st century for the 4.5 (RCP4.5) and 8.5 (RCP8.5) representative concentration pathways. The RCP4.5 pathway did not show a consistent and significant trend in SAM. The RCP8.5 pathway, however, showed a significant and positive trend in SAM that varied from 0.01 yr^{-1} to 0.06 yr^{-1} for different models. Using an average trend in SAM of 0.03 yr^{-1}, and based on point-wise linear relation between annual SAMI and Chl obtained by regression using the MODIS data in 2000–2018, the surface Chl change over the next 50 years was projected for the NAP and WAP regions, which varies from 0 to 0.5 mg m^{-3} (Fig. 15a). Projected change in Chl-100m associated with SAM

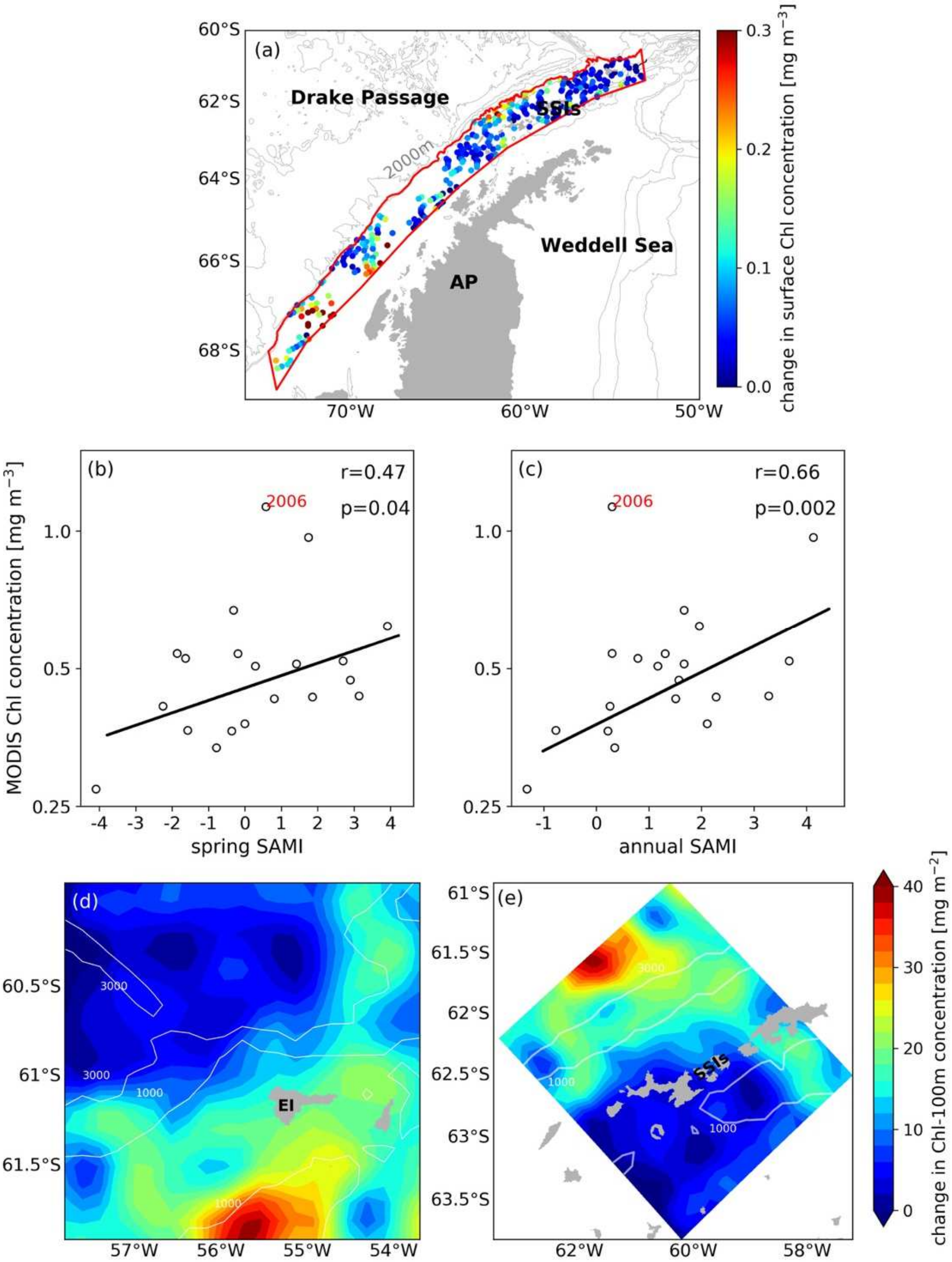

Fig. 15. (a) Map showing the portion of the western Antarctic Peninsula outer shelf and slope (red outline) that was used for projection of change in surface chlorophyll concentration over the next 50 years (colored circles), assuming a SAM trend of 0.03 yr^{-1}. Only locations with significant correlations ($p<0.1$) between surface chlorophyll concentration and annual SAMI for 2000–2018 (MODIS period) are shown. (b) Regression between area-averaged surface chlorophyll concentration over the selected region versus the spring SAMI for 2000 to 2018 (solid line). The correlation coefficient (r) and significance level (p) of the correlation are shown. (c) Same as (b) except for annual SAMI. Projected change in chlorophyll concentration integrated over the upper 100 m in the next 50 years for the (d) Elephant Island (EI) and (e) South Shetland Islands (SSIs) regions.

over the next 50 years for the EI region varies from 10–25 mg m^{-2} over the continental shelf region inshore of the 1000-m isobath to 30–50 mg m^{-2} in deeper ocean south of EI (Fig. 15d). In the SSIs region, significant change in Chl-100m occurs north of the SSIs and varies from 10 mg m^{-2} to over 40 mg m^{-2} (Fig. 15e). These projections are only valid if the SAM-Chl relationship is robust over the next 50 years, and if such a relationship includes future decadal variability, such as that observed between SAM and physical variables (e.g., MLD, CDW extent) for 1990–2010, the projected change in Chl concentration needs to be re-evaluated.

5. Conclusions

The long-term hydrographic and chlorophyll measurements made by the U.S. AMLR program during the austral summer near EI and the SSIs captured decadal variability in the relationships between the NAP ocean environment and large-scale climate modes. The interannual variations in hydrographic properties and chlorophyll concentration in the AMLR study area are significantly and positively correlated with SAM post 2000, with weak or insignificant correlation before 2000. The AMLR observations are one of the longest time series for Antarctic coastal and shelf waters and these are just at the resolution of decadal climate variability. This underscores the importance of maintaining long term measurement programs in the Antarctic. The SAM-chlorophyll production relationship in the study area is opposite to that found in the northern part of the west Antarctic Peninsula continental shelf, suggesting different roles across the Antarctic ocean of vertical mixing in regulating natural iron input to the marine ecosystem that are associated with a change in SAM.

The projected chlorophyll response to SAM in the EI and SSIs regions suggest significant increase in phytoplankton production. Assuming the other correlations with SAM persist, then the shift to longer periods of positive SAM in the EI and SSIs regions will be accompanied by enhanced vertical mixing, increased irradiance availability, and increased CDW inputs; all of which support increased primary production. These regions support diverse and productive food webs. Enhanced chlorophyll biomass will potentially manifest itself in greater standing stocks throughout the food web. However, it is unknown what effect vertical mixing changes will have on the phytoplankton composition, which can be an important factor in regulating grazing and energy transfer within food webs. In other polar systems like the Ross Sea, future changes have been modeled, and it was suggested that phytoplankton composition will respond to the environmental forcing (mixed layer depth changes, iron inputs, sea ice removal) and also change (Smith et al., 2014; Kaufman et al., 2017). The importance of similar changes in the West Antarctic remains uncertain, and awaits a clear description of the mechanisms that influence phytoplankton composition in this region.

Acknowledgement

Support for Z. Zhang and M. Zhou was provided by the National Natural Science Foundation of China (grant number 41876221 and grant number 41941008). Support for M. Dinniman and E. Hofmann was provided by U.S. National Science Foundation grant OPP-1643652. Support for W. Smith Jr. was provided by the National Natural Science Foundation of China (grant number 41876228). We thank the two anonymous reviewers for their helpful comments that substantially improved the manuscript.

References

Ardelan, M.V., Holm-Hansen, O., Hewes, C.D., Reiss, C.S., Silva, N.S., Dulaiova, H., Steinnes, E., Sakshaug, E., 2010. Natural iron enrichment around the antarctic Peninsula in the Southern Ocean. Biogeosciences 7 (1), 11–25.

Alderkamp, A.-C., Mills, M.M., van Dijken, G.L., Laan, P., Thuroczy, C.-E., Gerringa, L., de Baar, H.J.W., Payne, C.D., Visser, R.J.W., Buma, A.G.J., Arrigo, K.R., 2012. Iron from melting glaciers fuels phytoplankton blooms in Amundsen Sea (Southern Ocean), Phytoplankton characteristics and productivity. Deep-Sea Res. II, 71–76, 32–48.

Annett, A.L., Skiba, M., Henley, S.F., Venables, H.J., Meredith, M.P., Statham, P.J., Ganeshram, P.J., 2015. Comparative roles of upwelling and glacial iron sources in Ryder Bay, coastal western Antarctic Peninsula. Mar. Chem. 176, 21–23.

Arblaster. J.M., Meehl, G.A., 2006. Contributions of external forcings to southern annular mode trends. J. Clim. 19, 2896–2905.

Arrigo, K.R., Mills, M.M., Kropuenske, L.R., van Dijken, G.L., Alderkamp, A.C., Robinson, D.H., 2010. Photophysiology in two major southern ocean phytoplankton taxa: photosynthesis and growth of Phaeocystis antarctica and Fragilariopsis cylindrus under different irradiance levels. Integr. Comp. Biol. 50(6), 950–966.

Arrigo, K. R., van Dijken, G.L., Alderkamp, A.-C., Erickson, Z.K., Lewis, K.M., Lowry, K.E., Joy-Warren, H.L., Middag, R., Nash-Arrigo, J.E., Selz., V., van de Poll, W., 2017. Early spring phytoplankton dynamics in the western Antarctic Peninsula. . J. Geophys. Res., 122, 9350–9369.

Ciasto, L.M., Simpkins, G.R., England, M.H., 2015. Teleconnections between Tropical Pacific SST Anomalies and Extratropical Southern Hemisphere Climate. J. Clim. 28, 56–65.

Dinniman, M.S., Klinck, J.M., 2004. A model study of circulation and cross-shelf exchange on the west Antarctic Peninsula continental shelf. Deep-Sea Res. II 51, 2003–2022.

Dinniman, M.S., Klinck, J.M., Hofmann, E.E., 2012. Sensitivity of Circumpolar Deep Water transport and ice shelf basal melt along the West Antarctic Peninsula to changes in the winds. J. Clim. 25, 4799–4816.

Dong, S., Sprintall, J., Gille, S., Talley, L., 2008. Southern Ocean mixed layer depth from Argo float profiles. J. Geophys. Res. 113, C06013.

Dotto, T.S., Kerr, R., Mata, M.M., Garcia, C.A.E., 2016. Multidecadal freshening and lightening in the deep waters of the Bransfield Strait, Antarctica. J. Geophys. Res. 121, 3741–3756.

Du, G., Zhang, Z., Zhou, M., Zhu, Y., Zhong, Y., 2018. The upper 1000-m slope currents north of the South Shetland Islands and Elephant Island based on ship cruise observations. J. Ocean Univ. China 17(2), 1091–1103.

Espinasse, B., Zhou, M., Zhu, Y., Hazen, E.L., FriedLaender, A.S., Nowacek, D.P., Chu, D., Carlotti, F., 2012. Austral fall winter transition of mesozooplankton assemblages and krill aggregations in an embayment west of the Antarctic Peninsula. Mar. Ecol. Prog. Ser. 452, 63–80.

Fach, B.A., Klinck, J.M., 2006. Transport of Antarctic krill (Euphausia superba) across the Scotia Sea. Part I: Circulation and particle tracking simulations. Deep-Sea Res. II 51, 987–1010.

Frants, M., Gille, S.T., Hatta, M., Hiscock, W.T., Kahru, M., Measures, C.I., Mitchell, B.G., Zhou, M., 2013. Analysis of horizontal and vertical processes contributing to natural iron supply in the mixed layer in southern Drake Passage. Deep-Sea Res. II 90, 68–76.

Gerringa, L.J.A., Alderkamp, A.-C., Laan, P., Thuróczy, C.-E., De Baar, H.J.W., Mills, M.M., Van Dijken, G.L., Van Haren, H., Arrigo, K.R., 2012. Iron from melting glaciers fuels the phytoplankton blooms in Amundsen Sea (Southern Ocean); iron biogechemistry. Deep-Sea Res. II 71–76, 16–31.

Gordon, A.L., Mensch, M., Dong, Z., Smethie, Jr, W.M., de Bettencourt J., 2000. Deep and bottom water of the Bransfield Strait eastern and central basins. J. Geophys. Res. Oceans,105(C5), 11337–11346.

Graham, J.A., Dinniman, M.S., Klinck, J.M., 2016. Impact of model resolution for on-shelf heat transport along the West Antarctic Peninsula. J. Geophys. Res. Oceans 121, 7880–7897.

Hamre, B., Stamnes, J.J., Frette, Ø, Erga, S., Stamnnes, K., 2008. Could stratospheric ozone depletion lead to enhanced aquatic primary production in the polar regions? Limnol. Oceanogr., 53(1), 332–338.

Jiang, M., Measures, C.I., barbeau, K., Charette, M.A., Gille, S.T., Hatta, M., Kahru, M., Mitchell, B.G., Naveira Garabato, A.C., Reiss, C., Selph, K., Zhou, M., 2019. Fe sources and transport from the Antarctic Peninsula shelf to the southern Scotia Sea. Deep-Sea Res. I 150, 103060.

Joy-Warren, H., van Dijken, G.L., Alderkamp, A., Leventer, A., Lewis, K.M., Selz, V., Lowry, K.E., van de Poll, W., Arrigo, K.A., 2019. Light is the primary driver of early season phytoplankton production along the western Antarctic Peninsula. J. Geophys. Res. Oceans 124(11), 7345–7399.

Kaufman, D.E., Friedrichs, M.A.M., Smith Jr., W.O., Hofmann, E.E., Dinniman, M.S., Hennings, J.C.P., 2017. Climate change impacts on Ross Sea biogeochemistry: results from 1D modeling experiments. J. Geophys. Res. 122, 2339–2359.

Lefebvre, W., Goosse, H., Timmermann, R., Fichefet, T., 2004. Influence of the Southern Annular Mode on the sea ice-ocean system. J. Geophys. Res. 109, C09005.

Li, X., Gerber, E.P., Holland, D.M., Yoo, C., 2015. A Rossby wave bridge from the tropical Atlantic to West Antarctica. J. Clim. 28(6), 2256–2273.

Loeb, V., Hofmann, E.E., Klinck, J.M., Holm-Hansen, O., 2010. Hydrographic control of the marine ecosystem in the South Shetland-Elephant Island and Bransfield Strait region. Deep-Sea Res. II 57, 519–542.

Marshall, G.J., 2003. Trends in the Southern Annular Mode from observations and reanalyses. J. Clim. 16, 4134–4143.

Martinson, D.G., Stammerjohn, S.E., Iannuzzi, I.A., Smith, R.C., Vernet, M., 2008. Western Antarctic Peninsula physical oceanography and spatio–temporal variability. Deep-Sea Res. II 55, 1964–1987.

Measures, C.I., Brown, M.T., Selph, K.E., Apprill, A., Zhou, M., Hatta, M., Hiscock, W.T., 2013. The influence of shelf processes in delivering dissolved iron to the HNLC waters of the Drake Passage, Antarctica. Deep-Sea Res. II 90, 77–88.

Murphy, E.J., Thorpe, S.E., Watkins, J.L., Hewitt, R., 2004. Modeling the krill transport pathways in the Scotia Sea: spatial and environmental connections generating the seasonal distribution of krill. Deep-Sea Res. II 51(12-13), 1435–1456.

Murphy, E.J., Watkins, J.L., Reid, K., Trathan, P.N., Everson, I., Croxall, J.P., Priddle, J., Brandon, M.A., Brierley, A.S., Hofmann, E., 1998. Interannual variability of the South Georgia marine ecosystem: biological and physical sources of variation in the abundance of krill. Fisheries Oceanography 7(3 - 4), 381 - 390.

Nowacek, D.P., Friedlaender, A.S., Halpin, P.N., Hazen, E.L., Johnston, D.W., Read, A.J., B. Espinasse, M. Zhou, Y. Zhu, 2011. Super-aggregations of krill and humpback whales in Wilhelmina Bay, Antarctic Peninsula. PLoS ONE 6(4), e19173.

Polvani, L.M., Waugh, D.W., Correa, G.J.P, Son, S.W., 2011. Stratospheric ozone depletion: the main driver of twentieth-century atmospheric circulation changes in the southern hemisphere. J. Clim. 24, 795–812.

Prézelin, B.B., Hofmann, E.E., Mengelt, C., Klinck, J.M., 2000. The linkage between Upper Circumpolar Deep Water (UCDW) and phytoplankton assemblages on the west Antarctic Peninsula continental shelf. J. Mar. Res. 58, 165–202.

Prézelin, B.B., Hofmann, E.E., Moline, M., Klinck, J.M., 2004. Physical forcing of phytoplankton community structure and primary production in continental shelf waters of the western Antarctic Peninsula. J. Mar. Res. 62, 419–460.

Reiss, C.S., Hewes, C.D., Holm-Hansen, O., 2009. Influence of atmospheric teleconnections and Upper Circumpolar Deep Water on phytoplankton biomass around Elephant Island, Antarctica. Mar. Ecol. Prog. Ser. 377, 51–62.

Renner, A.H.H., Thorpe, S.E., Heywood, K.J., Murphy, E.J., Watkins, J.L., Meredith, M.P., 2012. Advective pathways near the tip of the Antarctic Peninsula: Trends, variability and ecosystem implications. Deep-Sea Res. I 63, 91–101.

Ruiz Barlett, E.M., Tosonotto, G.V., Piola, A.R., Sierra, M.E., Mata, M.M., 2018. On the temporal variability of intermediate and deep waters in the Western Basin of the Bransfield Strait. Deep-Sea Res. II 149, 31–46.

Saba, G.K., Fraser, W.R., Saba, V.S., lannuzzi, R.A., Coleman, K.E., Doney, S.C., Duckflow, H.W., Martinson, D.G., Miles, T.N., Patterson-Fraser, D.L., Stammerjohn, S.E., Steinberg, D.K., Schofield, O.M., 2014. Winter and spring controls on the summer food web of the coastal West Antarctic Peninsula. Nat. Commun. 5, 4318.

Schmidtko, S., Heywood, K.J., Thompson, A.F., Aoki, S., 2014. Multidecadal warming of Antarctic waters. Science 346 (6214), 1227–1231.

Schofield, O., Brown, M,. Kohut, J., Nardelli, S., Saba, G., Waite, N., Ducklow, H., 2018. Changes in the upper ocean mixed layer and phytoplankton productivity along the West Antarctic Peninsula. Phil. Trans. R. Soc. A 376, 20170173.

Sen Gupta, A., England, M.H., 2006. Coupled ocean–atmosphere–ice response to variations in the southern annular mode. J. Clim. 19, 4457–4486.

Serebrennikova, Y.M., Fanning, K.A., 2004. Nutrients in the Southern Ocean GLOBEC region: Variations, water circulation, and cycling, Deep-Sea Res. II 51, 1981–2002.

Shindell, D. T., Schmidt, G. A., 2004. Southern Hemisphere climate response to ozone changes and greenhouse gas increase. Geophys. Res. Lett. 31, L18209.

Simpkins, G.R., Ciasto, L.M., Thompson, D., England, M.H., 2012. Seasonal relationships between large-scale climate variability and Antarctic sea ice concentration. J. Clim. 19, 5451–5469.

Smith Jr., W.O., Ainley, D.G., Arrigo, K.R., Dinniman, M.S., 2014. The oceanography and ecology of the Ross Sea. Annu. Rev. Mar. Sci. 6, 469–487.

Stammerjohn, S.E., Martinson, D.G., Smith, R.C., Yuan, X., Rind, D., 2008. Trends in Antarctic annual sea ice retreat and advance and their relation to El Niño-Southern Oscillation and southern annular mode variability. J. Geophys. Res. 11, C03S90.

Tagliabue, A., Sallée, J., Bowie, A.R., Lévy, M., Swart, S., Boyd, P.W., 2014. Surface-water iron supplies in the Southern Ocean sustained by deep winter mixing. Nat. Geosci. 7, 314–320.

Thompson, D.W.J, Solomon, S., Kushner, P., England, M., Grise, K.M., Karoly, D., 2011. Signatures of the Antarctic ozone hole in Southern Hemisphere surface climate change. Nat. Geosci. 4, 741–749.

Turner, J., Colwell, S.R., Marshall, G.J., Lachlan-Cope, T.A., Carleton, A.M., Jones, P.D., Lagun, V., Reid, P.A., Iagovkina, I., 2005. Antarctic climate change during the last 50 years. Int. J. Climatol. 25, 279–294.

Yeo, S.R., Kim, K.Y., 2015. Decadal changes in the Southern Hemisphere sea surface temperature in association with El Niño–Southern Oscillation and Southern Annular Mode. Clim. Dyn. 45, 3227–3242.

Yu, J., Paek, H., Saltzman, E.S., Lee, T., 2015. The early 1990s change in ENSO–PSA–SAM relationships and its impact on Southern Hemisphere climate. J. Clim. 28, 9393–9408.

Zhang, Z., Uotila, P., Stössel, A., Vihma, T., Liu, H., Zhong, Y., 2018. Seasonal southern hemisphere multi-variable reflection of the southern annular mode in atmosphere and ocean reanalyses. Clim. Dyn. 50(3-4), 1451–1470.

Zheng, F., Li, J., Clark, R.T., Nnamchi, H.C., 2013. Simulation and projection of the southern hemisphere annular mode in CMIP5 models. J. Clim. 26, 9860–9879.

Zhou, M., Zhu, Y., Measures, C.I., Hatta, M., Charette, M.A., Gille, S.T., Frants, M., Jiang, M., Mitchell, B.G., 2013. Winter mesoscale circulation on the shelf slope region of the southern Drake Passage. Deep-Sea Res. II 90, 4–14.

Supplementary materials

Table S1. Coefficients and p values (numbers in parenthesis) of correlations between oceanic quantities in the EI and SSIs regions with SAM indices, and of correlations between Chl-100m and the physical factors. All statistics are for the period of 2001–2011.

	MLD		**PAR**	**T_{CDW}**		**Chl-100m**	
	EI	SSIs	EI	EI	SSIs	EI	SSIs
Summer SAMI	0.89	0.59	0.64[a]			0.71	0.59[b]
	(0.003)	(0.05)	(0.04)			(0.02)	(0.09)
Spring SAMI				0.57	0.75		0.64[c]
				(0.07)	(0.01)		(0.06)
Annual SAMI				0.56	0.71		0.78[c]
				(0.08)	(0.01)		(0.01)
MLD						0.60[a]	
						(0.07)	
PAR						0.75[a]	
						(0.01)	
T_{CDW}							0.54[c]
							(0.10)

[a]: Data from 2006 are excluded
[b]: Data from 2006 and 2008 are excluded
[c]: Data from 2006 and 2011 are excluded

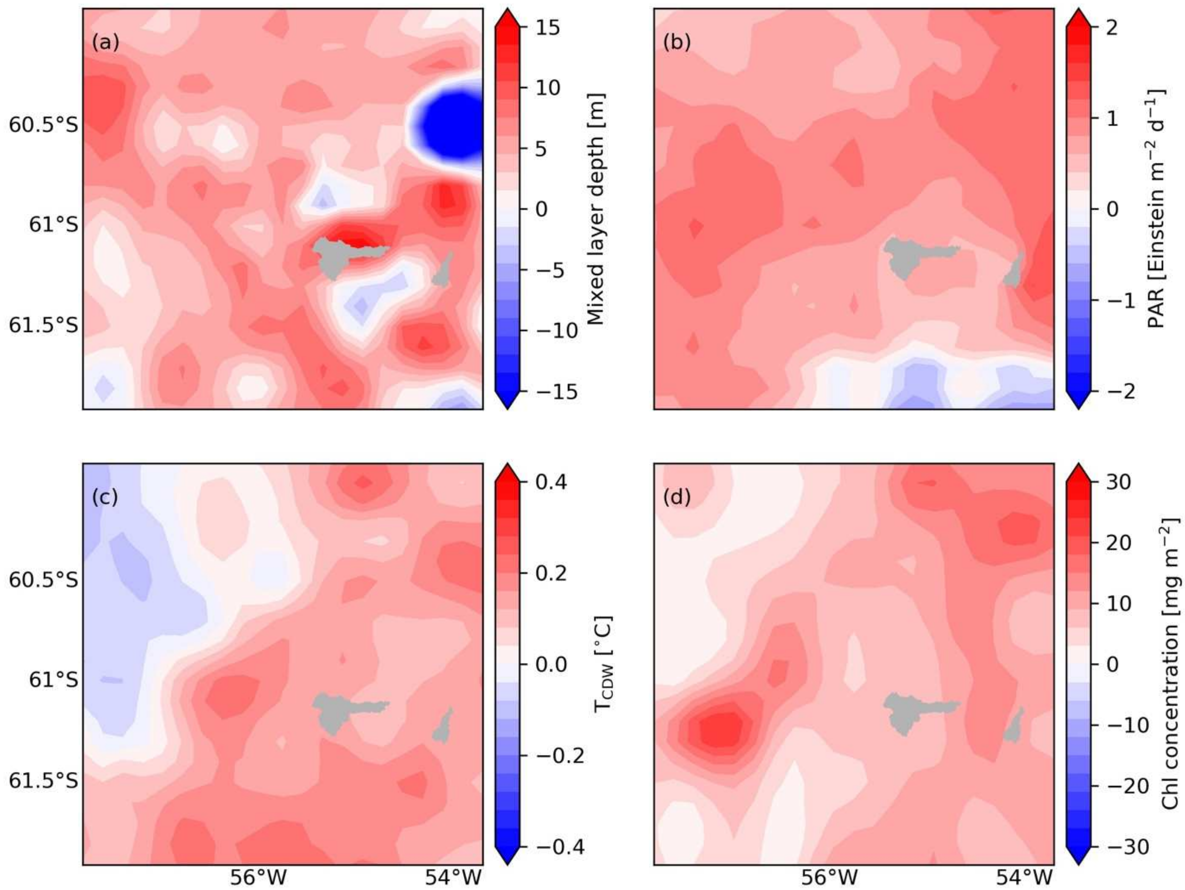

Fig. S1. The 1st EOF modes of (a) mixed layer depth, (b) photosynthetically available radiation (PAR), (c) temperature at the potential density surface of 27.6 kg m^{-3} (T_{CDW}) and (c) integrated Chl concentration over the upper 100 m for the Elephant Island region.

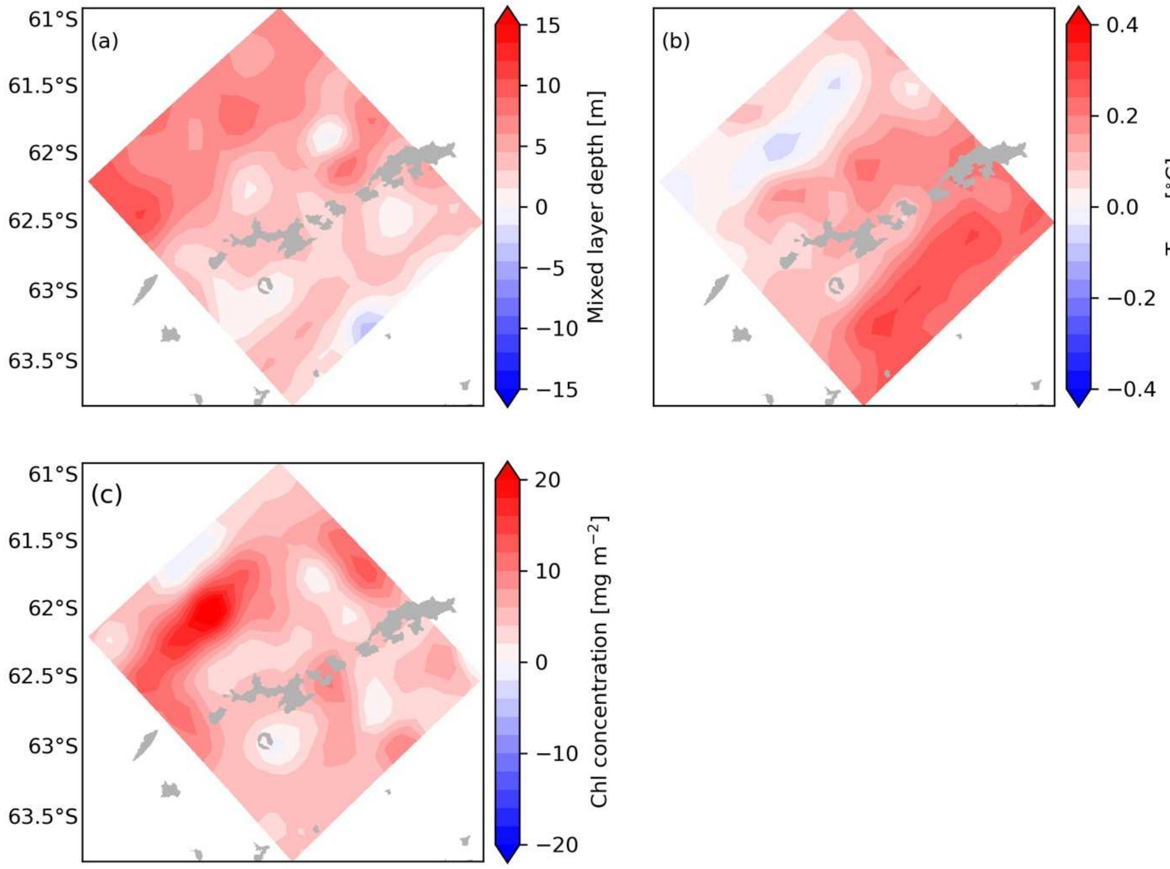

Fig. S2. The 1st EOF modes of (a) mixed layer depth, (b) temperature at the potential density surface of 27.6 kg m^{-3} (T_{CDW}) and (c) integrated Chl concentration over the upper 100 m for the South Shetland Islands region.